



1 **Suspended Particulate Matter drives the spatial segregation of** 2 **nitrogen turnover along the hyper-turbid Ems estuary**

3 Gesa Schulz^{1,2}, Tina Sanders¹, Justus E. E. van Beusekom^{2,3}, Yoana G. Voynova², Andreas Schöl⁴, Kirstin
4 Dähnke²

5 ¹Institute of Geology, Center for Earth System Research and Sustainability (CEN), University Hamburg, Hamburg, 20146,
6 Germany

7 ²Institute of Carbon Cycles, Helmholtz-Zentrum Hereon, Geesthacht, 21502, Germany

8 ³Institute of Oceanography, University Hamburg, Hamburg, 20146, Germany

9 ⁴Department of Microbial Ecology, Federal Institute of Hydrology, Koblenz, 56068, Germany

10

11 *Correspondence to:* Gesa Schulz (Gesa.Schulz@hereon.de)

12 **Abstract**

13 Estuaries are nutrient filters and change riverine nutrient loads before they reach coastal oceans. They have been extensively
14 changed by anthropogenic activities like draining, deepening, and dredging to meet economic and social demand, causing
15 significant regime changes like tidal amplifications and in some cases to hyper-turbid conditions. Furthermore, increased
16 nutrient loads, especially nitrogen, mainly by agriculture cause coastal eutrophication. Estuaries can either act as a sink or as
17 a source of nitrate, depending on environmental and geomorphological conditions. These factors vary along an estuary, and
18 change nitrogen turnover in the system. Here, we investigate the factors controlling nitrogen turnover in the hyper-turbid Ems
19 estuary (Northern Germany) that has been strongly impacted by human activities. During two research cruises in August 2014
20 and June 2020, we measured water column properties, dissolved inorganic nitrogen, dual stable isotopes of nitrate and
21 dissolved nitrous oxide concentration along the estuary. Overall, the Ems estuary acts as a nitrate sink in both years. However,
22 three distinct biogeochemical zones exist along the estuary. A strong fractionation (~ 26 ‰) of nitrate stable isotopes points
23 towards nitrate removal via water column denitrification in the hyper-turbid Tidal River, driven by anoxic conditions in deeper
24 water layers. In the Middle Reaches of the estuary nitrification gains in importance turning this section into a net nitrate source.
25 The Outer Reaches are dominated by mixing with nitrate uptake in 2020.
26 We find that the overarching control on biogeochemical nitrogen cycling, zonation and nitrous oxide production in the Ems
27 estuary is exerted by suspended particulate matter concentrations and the linked oxygen deficits.

28 **1 Introduction**

29 Estuaries can significantly alter riverine nutrient loads before they reach adjacent coastal oceans (Bouwman et al., 2013;
30 Crossland et al., 2005). Estuaries have been extensively altered by humans and anthropogenic activities to meet economic and
31 social demands. Draining, damming, diking, deepening and dredging lead to significant regime changes including tidal
32 amplification, hyper-turbid conditions and loss of habitats (e.g. Stronge et al. 2005; Winterwerp et al. 2013; De Jonge et al.



33 2014). High nutrient loads from agriculture, waste water and urban runoff have induced eutrophication (Galloway et al., 2003;
34 Howarth, 2008; Van Beusekom et al., 2019), one of the greatest threats to coastal ecosystems worldwide (e.g. Howarth and
35 Marino 2006; Voss et al. 2011).

36 Depending on predominant microbial processes, environmental conditions and geomorphological characteristics, estuaries can
37 either act as a sink or as an additional source of nitrate (Dähnke et al., 2008; Middelburg and Nieuwenhuize, 2001). Especially
38 the balance between remineralisation/nitrification and denitrification determines the net role of a specific estuary. Previous
39 studies found that biogeochemical changes of dissolved oxygen saturation, residence time or light penetration affect this
40 balance of nutrient uptake and removal (Carstensen et al., 2014; Diaz and Rosenberg, 2008; Thornton et al., 2007; Voss et al.,
41 2011).

42 To disentangle the role of nitrate production and removal processes, stable isotopes are a frequently used tool, because nitrogen
43 turnover processes usually discriminate versus heavier isotopes, leading to an enrichment in the pool of remaining substrate.
44 The magnitude of enrichment, the so-called isotope effect, is process-specific (e.g. Granger et al. 2004; Deutsch et al. 2006;
45 Sigman et al. 2009).

46 Nitrification and denitrification also produce nitrous oxide (N_2O) (Knowles, 1982; Tiedje, 1988; Wrage et al., 2001; Francis
47 et al., 2007), a potent greenhouse gas that contributes to global warming (IPCC, 2007). Estuaries are potential sources for
48 nitrous oxide (Bange, 2006) and, together with coastal wetlands, contribute approximately 0.17 to 0.95 Tg N_2O -N per year to
49 the global nitrous oxide budget of 16.9 Tg N_2O -N per year (Murray et al., 2015; Tian et al., 2020). Numerous factors control
50 estuarine nitrous oxide emissions. Oxygen depletion, nutrient levels and possibly organic matter composition trigger nitrous
51 oxide production. Therefore, nitrous oxide emissions is linked to eutrophication (e.g. de Wilde and de Bie 2000; Galloway et
52 al. 2003; Murray et al. 2015; Quick et al. 2019). The role of nitrous oxide production can vary along an estuary, depending on
53 the environmental and geomorphological properties.

54 Although the individual nitrogen turnover processes are well understood, the interplay of multiple stressors on the nitrogen
55 cycle needs further investigation (e.g. Billen et al. 2011; Giblin et al. 2013; Sanders and Laanbroek 2018). Therefore, we
56 investigate how water column properties can change the nitrogen turnover, emerging eutrophication and nitrous oxide
57 production along an estuary.

58 We performed two research cruises along the Ems estuary, a heavily managed estuary in Germany that underlies anthropogenic
59 pressures from fertilizer input, dredging, and channel deepening (De Jonge, 1983; Talke and de Swart, 2006; Johannsen et al.,
60 2008) leading to a significant increase of suspended particulate matter concentration in the inner estuary (De Jonge et al.,
61 2014). We studied water column nutrient and stable isotope composition, as well as suspended particulate matter properties in
62 the Ems estuary to investigate spatial dynamics in nitrogen removal, nitrogen turnover processes and their relation to nitrous
63 oxide production. We have (1) evaluated the zonation of nitrogen turnover along the estuary, (2) identified the dominating
64 nitrogen turnover pathways in individual zones, and (3) discussed the controlling factors of nitrogen cycling and emerging
65 nitrous oxide production. Ultimately, with this study we provide a better insight into the effects of water column properties
66 and biogeochemistry on estuarine nutrient turnover.



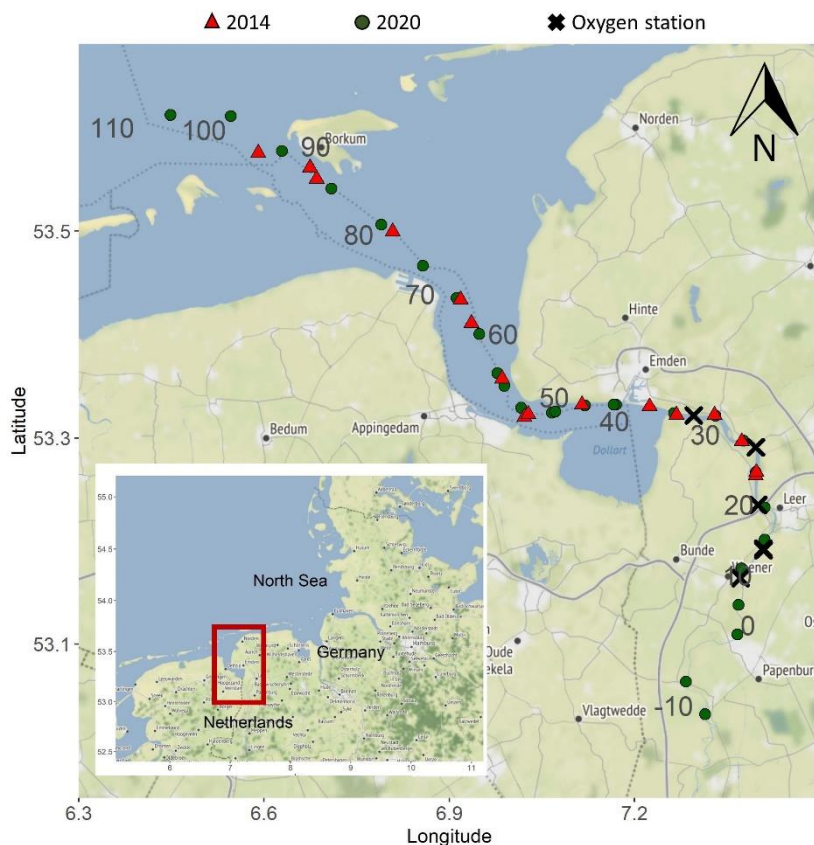
67 2 Methods

68 2.1 Study site

69 The Ems estuary is situated on the Dutch-German border (Fig.1). The estuary is approximately 100 km long and stretches from
70 the weir at Herbrum to the island Borkum. The Ems discharges into the Wadden Sea, a part of the southern North Sea (Van
71 Beusekom and de Jonge, 1994). The catchment of the Ems is 17 934 km² (Krebs and Weilbeer, 2008) and is densely populated,
72 with 86 % urban/agricultural land-use (Johannsen et al., 2008). The Ems is also an important waterway with ports in Delfzijl
73 and Emden, and is used for transport of large vessels from the shipyard in Papenburg to the North Sea (Talke and de Swart,
74 2006).

75 The Ems is characterized by steep gradients in salinity and tides (Compton et al., 2017). It has an average discharge of
76 80.8 m³ s⁻¹, with low fresh water discharge in summer, and highest discharge between January and April. The Ems is a hyper-
77 turbid estuary with high suspended sediment concentrations (De Jonge et al., 2014; Van Maren et al., 2015b), reaching values
78 of up to 30-40 g L⁻¹ and more in fluid mud layers (Winterwerp et al., 2013). Channel deepening has led to tidal amplification
79 and an increased upstream sediment transport in the tidal Ems (De Jonge et al., 2014). The increase of suspended matter
80 lowered light penetration, and led to decreasing oxygen concentration (Bos et al., 2012). Bos et al. (2012) classified the Ems
81 estuary as a degraded ecological system with high nutrient loads.

82 Based on geomorphological characteristics, the Ems can be divided into four sections: the Tidal River (km 14–km 35), Dollard
83 Reach (km 35–km 43), Middle Reaches (km 43–km 75) and Outer Reaches (downstream from km 75) (Fig. 1).



84

85 **Figure 1:** Map of the Ems estuary displaying the sampling stations. Red triangles mark stations done in 2014, green points stations
86 in 2020 and crosses show oxygen measurements stations. The grey numbers show the stream kilometers calculated according to
87 German federal waterways (wsv.de). Background map: © OpenStreetMap contributors 2021. Distributed under the Open Data
88 Commons Open Database License (ODbL) v1.0.

89 2.2 Sampling

90 Water samples were taken during two research cruises with the research vessel *Ludwig Prandtl* in August 2014 and June 2020.
91 Nutrient concentration and suspended particulate matter concentration from the cruise in 2014 have been published in Sanders
92 and Laanbroek (2018). An onboard membrane pump provided the on-line in-situ FerryBox system with water from 2 m below
93 the surface. The FerryBox system continuously measures dissolved oxygen, water temperature, pH, salinity, fluorescence and
94 turbidity (Petersen et al., 2011). In 2014, the dissolved oxygen measurements from the FerryBox were about $32 \mu\text{mol L}^{-1}$ lower
95 than the Winkler titrations of two discrete samples collected in July 2014. This offset was used to correct the FerryBox optode
96 measurements. Salinity measurements were checked using Optimare Precision Salinometer (Bremerhaven, Germany), and the
97 error of the FerryBox measurements was within 0.01 salinity units.
98 Discrete water samples were taken from a bypass of the FerryBox system. The samples for nutrient and isotope analysis were
99 filtered immediately through combusted, pre-weighted GF/F Filters (4 h, 450°C), and stored frozen in acid-washed (10 %



100 HCl, overnight) PE-Bottles at -20 °C until analyses. The filters were stored at -20 °C for later analysis of suspended particulate
101 matter (SPM) (Röttgers et al., 2014), $\delta^{15}\text{N}$ -SPM and C/N ratios. C/N ratios were measured with an Elemental Analyzer
102 (Eurovector EA 3000) calibrated against a certified acetanilide standard (IVA Analysentechnik, Germany). The standard
103 deviation was 0.05 % and 0.005 % for carbon and nitrogen respectively. During the 2020 cruise, nitrous oxide gas phase mole
104 fractions were continuously measured in unfiltered water.

105 2.2 Dissolved oxygen measurements

106 During the cruises in 2014 and 2020, we measured dissolved oxygen concentration in surface water using the FerryBox system
107 (see above). For a more detailed view on oxygen dynamics, we also used data provided by the German Federal Institute of
108 Hydrology (Bundesanstalt für Gewässerkunde – BfG) (BfG, unpublished). Vertical profiles of oxygen concentration were taken
109 at four monitoring stations along the Ems estuary (Fig. 1) in August 2014 and June 2020 using an YSI 6660 probe. At these
110 stations, oxygen and temperature were also continuously measured with miniDot® (PME, Precision Measurement
111 Engineering) loggers at 0.5 m above the bottom at Ems kilometer 11.8 and 24.5 in 2014 and additionally at 18.2 and 33.0 in
112 2020.

113 2.3 Nutrient measurements

114 Nutrient concentration (nitrate, nitrite, ammonium, silicate and phosphate) was measured with a continuous flow auto analyzer
115 (AA3, SEAL Analytics) using standard colorimetric and fluorometric techniques (Hansen and Koroleff, 2007). Measurement
116 ranges were 0-400 $\mu\text{mol-N L}^{-1}$ for combined nitrate and nitrite, 0-17.8 $\mu\text{mol-N L}^{-1}$ for nitrite, 0.07-25 $\mu\text{mol-N L}^{-1}$ for
117 ammonium, 0-1000 $\mu\text{mol-Si L}^{-1}$ for silicate and 0-16.1 $\mu\text{mol-P L}^{-1}$ for phosphate.

118 2.4 Isotopic analysis

119 The stable isotope composition of nitrate ($\delta^{15}\text{N}$ - NO_3^- , $\delta^{18}\text{O}$ - NO_3^-) was measured using the denitrifier method (Sigman et al.,
120 2001; Casciotti et al., 2002), which is based on the isotopic analysis of nitrous oxide. In brief, *Pseudomonas aureofaciens*
121 (ATCC#13985) reduce nitrate and nitrite⁻ in the filtered water samples to nitrous oxide. Nitrous oxide was measured by a
122 GasBench II coupled with an isotope ratio mass spectrometer (Delta Plus XP, Thermo Fisher Scientific). Two international
123 standards (USGS34, $\delta^{15}\text{N}$ - NO_3^- -1.8 ‰, $\delta^{18}\text{O}$ - NO_3^- -27.9 ‰; IAEA, $\delta^{15}\text{N}$ - NO_3^- +4.7 ‰, $\delta^{18}\text{O}$ - NO_3^- +25.6 ‰) and one internal
124 standard ($\delta^{15}\text{N}$ - NO_3^- +7.6 ‰, $\delta^{18}\text{O}$ - NO_3^- +24.4 ‰) were used to calibrate the samples. The standard deviation for standards
125 and samples was <0.2 ‰ (n= 4) and <0.5 ‰ (n=4) for $\delta^{15}\text{N}$ - NO_3^- and $\delta^{18}\text{O}$ - NO_3^- respectively. Nitrite concentration of the
126 samples was usually <5 ‰. When nitrite exceeded 5 ‰, it was removed prior to analysis using Sulfamic Acid (Granger and
127 Sigman, 2009).

128 An Elemental analyzer (Carlo Erba NA 2500) coupled with an isotope ratio mass spectrometer (Finnigan MAT 252) was used
129 to measure $\delta^{15}\text{N}$ -SPM values. IAEA N1 ($\delta^{15}\text{N}$ = +0.4 ‰), IAEA N2 ($\delta^{15}\text{N}$ = +20.3 ‰) and a certified sediment standard (IVA
130 Analysentechnik, Germany) were used as reference materials.



131 2.5 Equilibrator based nitrous oxide measurements and calculations

132 An nitrous oxide analyzer (Model 914-0022, Los Gatos Res. Inc.) coupled with a sea water/gas equilibrator measured the dry
133 mole fraction of nitrous oxide and water vapor in the water column using off-axis integrated cavity output spectroscopy. The
134 set-up and instrument precision is described in detail in Brase et al. (2017). The equilibration time of nitrous oxide of
135 approximately 7 min was taken into account for data processing.

136 For validation of the measurements, we measured two standard gas mixtures of nitrous oxide in synthetic air regularly (500.5
137 ppb \pm 5 % and 321.2 ppb \pm 3 %). No drift was detected. For further data processing, we calculated 1 min averages of nitrous
138 oxide detected dry mole fraction (ppm). We calculated the dissolved nitrous oxide concentration in water (N_2O_{cw}) using the
139 Bunsen solubility function of Weiss and Price (1980) taking temperature differences between sample inlet and equilibrator
140 into account (Rhee et al., 2009). Nitrous oxide saturation (s) was calculated using Eq. (1), based on nitrous oxide concentration
141 in water (N_2O_{cw}) and atmospheric nitrous oxide (N_2O_{air}).

$$142 \quad s = 100 \times \frac{N_2O_{cw}}{N_2O_{air}} \quad (1)$$

143 Atmospheric nitrous oxide was measured regularly during our cruise and was on average 0.33 ppm during our cruise in 2020.
144 The gas transfer coefficient (k) was calculated based on Borges et al. (2004), where u_{10} is wind speed 10 m above surface, and
145 Sc is the Schmidt number (Eq. (2)). Sea-to-air flux densities were calculated using Eq. (3).

$$146 \quad k = 0.24 \times (4.045 + 2.58u_{10}) \times \left(\frac{Sc}{600}\right)^{-0.5} \quad (2)$$

$$147 \quad f = k \times (N_2O_{cw} - N_2O_{air}) \quad (3)$$

148 2.5 Nitrate mixing calculations

149 Nitrate concentration from conservative mixing (C_{Mix}) between two endmembers was calculated for each sample using the
150 classical mixing model of Liss (1976).

$$151 \quad C_{Mix} = f \times C_R + (1 - f)C_M \quad (4)$$

152 Where C_R and C_M stand for the concentration of the riverine and marine end-members, respectively, and f denotes freshwater
153 fractionation in each sample calculated as follows:

$$154 \quad f = \frac{(S_M - S_{Mix})}{(S_M - S_R)} \quad (5)$$

155 S_{Mix} , S_M , S_R denote the salinity of the sample, marine and riverine endmembers, respectively. We used the concentration-
156 weighted mean of the isotopic values of the marine (δ_M) and riverine (δ_R) end-members to calculate the theoretical isotope
157 value of samples following conservative mixing (δ_{Mix}) (Fry, 2002):



$$\delta_{Mix} = \frac{f \times C_R \times \delta_R + (1-f) \times C_M \times \delta_M}{C_{Mix}} \quad (6)$$

159 2.6 Isotope effect

160 During turnover processes, nitrogen isotopes ratios change along a specific isotope effect that helps to identify individual
161 process pathways (e.g. Kendall et al. 2007). Isotope effects were calculated with an open-system approach where the reactant
162 nitrate is continuously supplied and partially consumed, and steady state is assumed. This leads to a linear relationship between
163 isotope values of nitrogen and fraction f , where $f = ([C]/[C_{initial}])$. The isotope effect ϵ corresponds to the slope of the regression
164 line (Sigman et al., 2009),

$$165 \epsilon_{substrate} = \frac{\delta^{15}N_{substrate} - \delta^{15}N_{initial}}{(1-f)} \quad (7)$$

$$166 \epsilon_{product} = \frac{\delta^{15}N_{product} - \delta^{15}N_{initial}}{f} \quad (8)$$

167 Where $\delta^{15}N_{substrate}$, $\delta^{15}N_{product}$, $\delta^{15}N_{initial}$ denote $\delta^{15}N$ values of the substrate and product at the time of sampling and the initial
168 value. The remaining fraction of substrate at the time of sampling is described by f . In the present study, the mixing line
169 determines initial concentrations and isotope values.

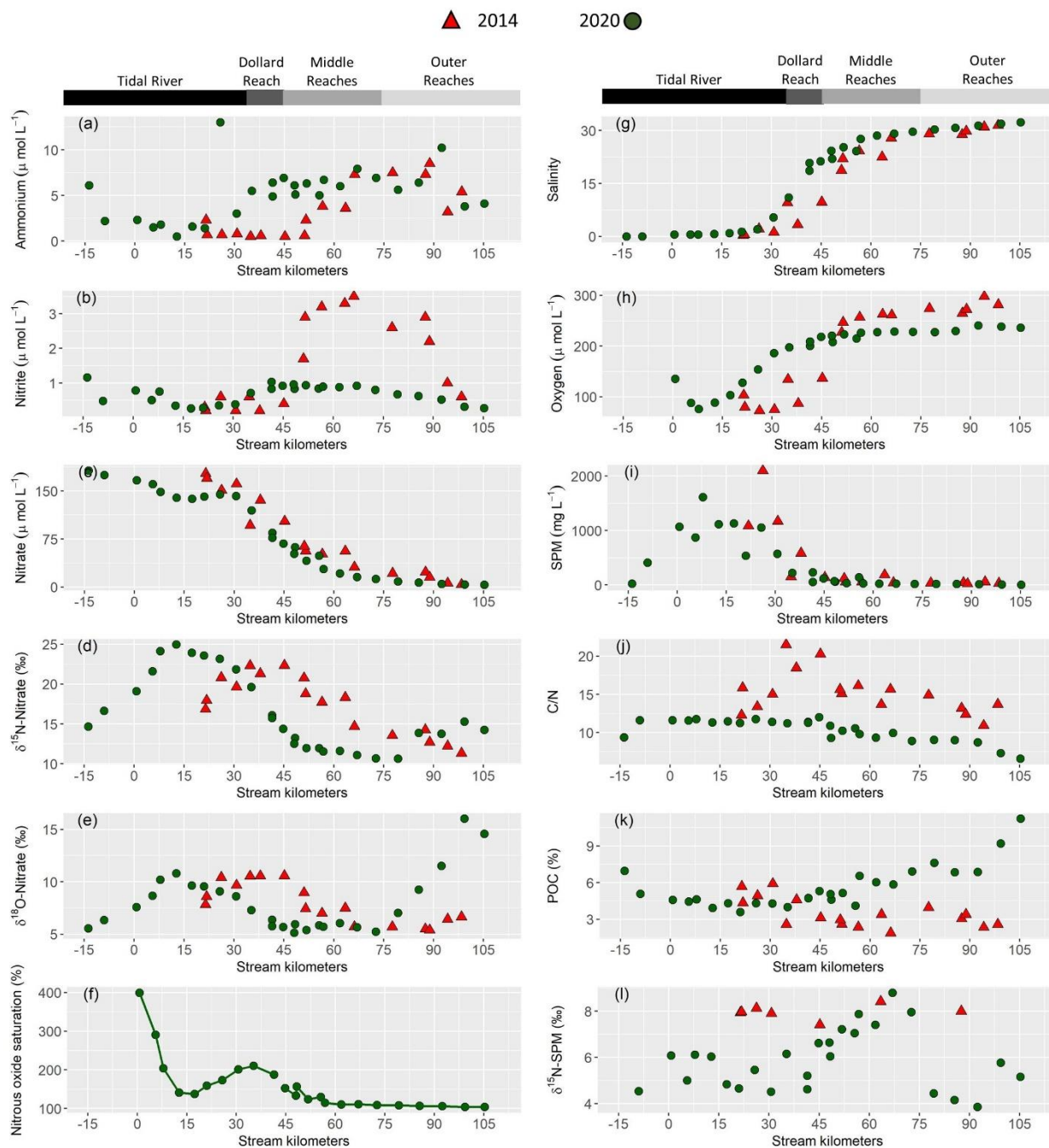
170 2.7 Statistical analysis

171 All statistical analysis were done using R packages. Pearson correlation matrices were calculated with ggcorr from the
172 R-package GGally v.2.0.0 (GGally: Extension to “ggplot2,” 2021). From the R-package stats v4.0.2 (The R Stats Package,
173 Version 4.0.2, 2021), we used the function prcomp for the principal component analysis (PCA). Salinity was not taken into
174 account for the multivariate analysis.

175 3 Results

176 3.1 Hydrographic properties and dissolved nutrients in surface water

177 To evaluate controls on nutrient cycling, we first regard the hydrochemical properties that were measured in 2014 and 2020 in
178 surface water, alongside with nutrient concentrations and nitrogen stable isotope composition (Fig. 2).



179

180 **Figure 2:** Near surface water column properties along the Ems estuary: (a) ammonium concentration in ($\mu\text{mol L}^{-1}$), (b) nitrite
 181 concentration in ($\mu\text{mol L}^{-1}$), (c) nitrate concentration in ($\mu\text{mol L}^{-1}$), (d) $\delta^{15}\text{N}$ -Nitrate in (‰), (e) $\delta^{18}\text{O}$ -Nitrate in (‰), (f) nitrous oxide
 182 saturation in (%), (g) salinity, (h) dissolved oxygen concentration in ($\mu\text{mol L}^{-1}$), (i) suspended particulate matter concentration (SPM) in
 183 (mg L^{-1}), (j) C/N ratios, (k) particulate organic carbon fraction (POC) in (%), (l) $\delta^{15}\text{N}$ -suspended particulate matter in (‰). Red triangles
 184 mark stations done in 2014 and green points stations in 2020.



185

186 Discharge ranged from $59.7 \text{ m}^3 \text{ s}^{-1}$ to $67.5 \text{ m}^3 \text{ s}^{-1}$ in 2014 and was $\sim 30 \text{ m}^3 \text{ s}^{-1}$ in 2020. The long-term average discharge is
187 $30\text{-}40 \text{ m}^3 \text{ s}^{-1}$ in June and August (NLWKN Bst. Aurich and Engels, 2021). The mean water temperature was $23 \text{ }^\circ\text{C}$ in 2014
188 and $17 \text{ }^\circ\text{C}$ in 2020. Salinity ranged from ~ 0.5 to ~ 32 in both years. In 2014, the sampling section started with the onset of the
189 salinity gradient (km 20), whereas the most upstream sample in 2020 was taken near Herbrum (km -14) (Fig. 2g), this and the
190 sample at stream kilometer -9 were taken by a bucket from the shore. The vessel based transect started in Papenburg (km 0).

191 Nitrate was the major form of dissolved inorganic nitrogen (DIN) and decreased with increasing salinity. Nitrate concentration
192 decreased from $177 \text{ } \mu\text{mol L}^{-1}$ to $3.9 \text{ } \mu\text{mol L}^{-1}$ in 2014 and from $166 \text{ } \mu\text{mol L}^{-1}$ to $4.9 \text{ } \mu\text{mol L}^{-1}$ in 2020 (Fig. 2c).

193 Ammonium (Fig. 2a) and nitrite (Fig. 2 b) concentration were generally low in the tidal river, with average concentrations of
194 ~ 3 and $1 \text{ } \mu\text{mol L}^{-1}$, respectively. One sample (June 2020, stream kilometer 25) had an unusually high ammonium concentration
195 of $13 \text{ } \mu\text{mol L}^{-1}$. In the Dollard Reach, ammonium and nitrite concentration increased with salinity in 2020, whereas this
196 increase occurred further downstream, i.e., in the Middle reaches, in 2014. The highest ammonium concentration was similar
197 in 2014 and 2020, with $8.5 \text{ } \mu\text{mol L}^{-1}$ and $10.2 \text{ } \mu\text{mol L}^{-1}$ respectively. Whereas in 2020 nitrite concentration reached $1 \text{ } \mu\text{mol L}^{-1}$,
198 with little variability along the transect, in 2014, it reached a maximum of $3.5 \text{ } \mu\text{mol L}^{-1}$ in a distinct peak in the Middle and
199 Outer Reaches.

200 Incoming nitrate isotope values were elevated in the most upstream regions of the Tidal River with values of 15 ‰ for
201 $\delta^{15}\text{N-NO}_3^-$ and 6 ‰ for $\delta^{18}\text{O-NO}_3^-$ in 2020, and 17 ‰ and 8 ‰ for $\delta^{15}\text{N-NO}_3^-$ and $\delta^{18}\text{O-NO}_3^-$ in 2014. Isotope values increased
202 further to a local maximum of 25 ‰ and 11 ‰ for $\delta^{15}\text{N-NO}_3^-$ and $\delta^{18}\text{O-NO}_3^-$ around km 13 in 2020. In 2014, the respective
203 local maxima (22 ‰ and 10 ‰ for $\delta^{15}\text{N-NO}_3^-$ and $\delta^{18}\text{O-NO}_3^-$) were shifted to km 35. Further downstream, isotope values
204 decreased, except for a slight increase in the outermost marine samples (Fig. 2d and Fig. 2e).

205 In 2020, we also measured dissolved nitrous oxide concentration. Measured values ranged between equilibrium concentrations
206 ($\sim 9 \text{ nmol L}^{-1}$) and supersaturation of up to 40 nmol L^{-1} at km 0, which corresponded to a saturation of 400 %. Nitrous oxide
207 then decreased downstream to $\sim 14 \text{ nmol L}^{-1}$ (140 %) at km 30 and then increased to a local maximum of $21 \text{ } \mu\text{mol L}^{-1}$ (210 %)
208 in the Tidal River/Dollard Reach transition at stream km 35. Further downstream, nitrous oxide decreased to near equilibrium
209 concentration towards the North Sea (Fig. 2f).

210 3.2 Suspended Particulate Matter properties

211 SPM concentration was highest in the Tidal River, reaching values of 2100 mg L^{-1} in 2014 and 1600 mg L^{-1} in 2020. SPM
212 concentration decreased at the beginning of the Dollard Reach region (Fig. 2i). The $\delta^{15}\text{N-SPM}$ values showed considerable
213 scatter (Fig. 2l): around 5 ‰ in the Tidal River/Dollard Reach, and 9 ‰ in the Middle Reaches. In the Outer Reaches,
214 $\delta^{15}\text{N-SPM}$ dropped again to ~ 5 ‰. In 2014, $\delta^{15}\text{N-SPM}$ were elevated (8 ‰), but the database during this cruise is relatively
215 sparse (Fig. 2l).



216 In 2020, C/N ratios of SPM (Fig. 2j) were relatively stable in the Tidal River (~11) and Dollard Reach, with a slightly lower
217 value of 9 in the most upstream sample. In the Middle Reaches, C/N ratios decreased, reaching the lowest value of 6.5 in the
218 most offshore sample. In 2014, C/N values were 11-15 in the Tidal River, increased to values as high as 20 in the Dollard
219 Reach and decreased to ~ 11 approaching the North Sea (Fig. 2j).

220 Particular organic carbon fraction (% POC) was high in the most upstream samples in 2020 (Fig. 2k), decreased to 4.5 % and
221 remained relatively stable in the Tidal River and Dollard before it increased in the Middle and Outer Reaches up to 11 %. In
222 2014, the values in Tidal River and Dollard were comparable, but we found a decreasing trend downstream, with a low POC
223 fraction of ~3 in the outermost sample (Fig. 2k).

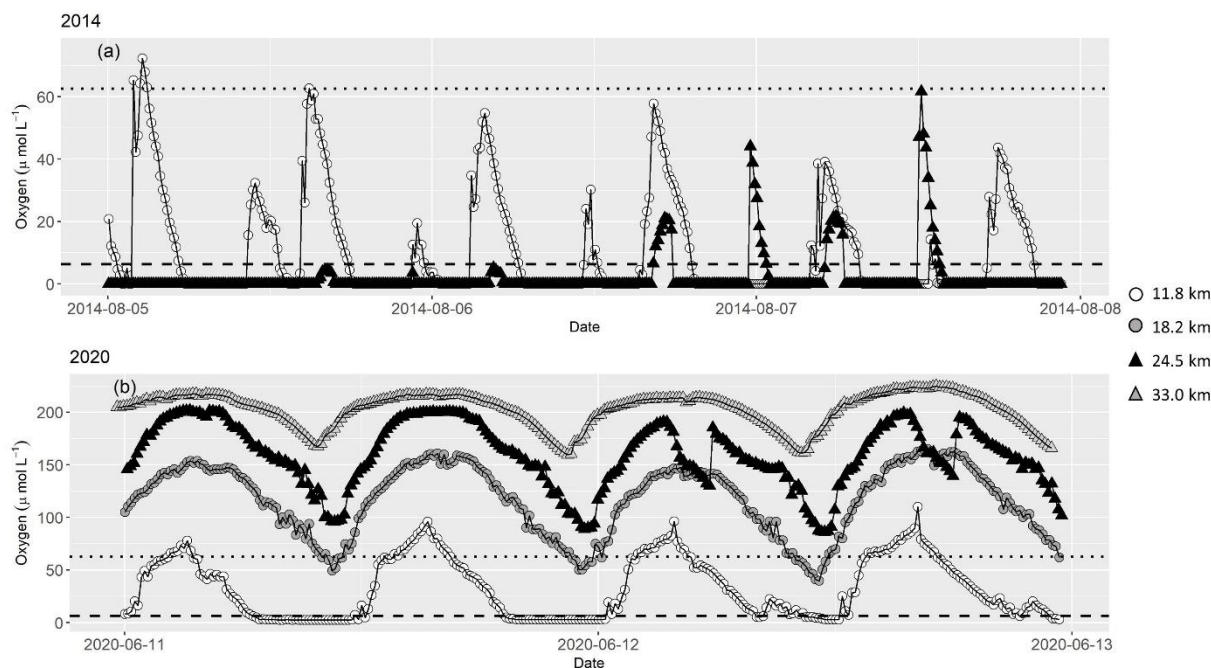
224 3.3 Dissolved oxygen concentration in the Ems estuary

225 In surface water, oxygen concentrations in the Tidal River section were low during both cruises, and increased downstream
226 with rising salinity. The lowest values were measured in the Tidal River, where the minimum oxygen concentration was
227 ~72 $\mu\text{mol L}^{-1}$ in 2014 and 76 $\mu\text{mol L}^{-1}$ in 2020 (Fig. 2h) corresponding to a saturation of 27 % and 26 % respectively.

228 Oxygen profiles showed strong vertical gradients with decreasing concentration in deeper water layers. The extent of hypoxia
229 in the water column depended on the tidal cycle and location, with lowest bottom water oxygen concentration measured at the
230 most upstream station at stream km 7.2 during low tide in 2020. Detailed profiles can be found in the supplementary material
231 (S1).

232 During the continuous near-bottom oxygen measurements, we found anoxic conditions during both of our cruises that lasted
233 for several hours over a tidal cycle (Fig. 3). Oxygen concentration was generally low at low tide, and elevated at high tide. In
234 2014, anoxia developed at stream km 11.8 and 18.5, and highest oxygen concentration in bottom water was only 60 $\mu\text{mol L}^{-1}$
235 (km 24.5) and 70 $\mu\text{mol L}^{-1}$ (km 11.8). At the beginning of August, oxygen concentration at kilometer 11.8 frequently exceeded
236 measured values at kilometer 24.5.

237 In 2020, oxygen concentration in bottom water was higher, and anoxia was only found at stream km 11.8. At all other stations,
238 oxygen concentration remained above 40 $\mu\text{mol L}^{-1}$ even at low tide.

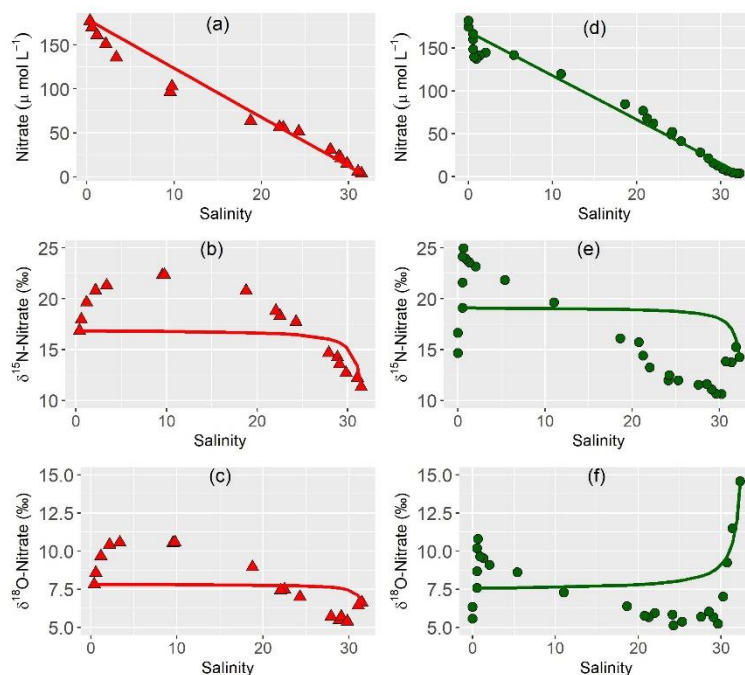


239

240 **Figure 3:** Dissolved oxygen concentration in ($\mu\text{mol L}^{-1}$) 0.5 m above riverbed during our research cruises in (a) 2014 and (b) 2020
241 measured continuously at several stations along the Tidal River. Point shapes and colors mark stream kilometer of each sampling station.
242 White points displaying results from a station at stream kilometer 11.8, grey at stream kilometer 18.2, black triangles at stream kilometer
243 24.5 and grey triangles at stream kilometer 33.0. The dotted line visualizes hypoxic conditions at oxygen concentration of $62.5 \mu\text{mol L}^{-1}$
244 (Diaz et al., 2019). The dashed line shows oxygen concentration ($6.25 \mu\text{mol L}^{-1}$) under which denitrification occurs (Seitzinger, 1988).
245 Plots (a) and (b) have different y-scales.

246 3.4 Nitrate mixing

247 We plotted salinity vs nitrate concentration and nitrate dual isotopes to evaluate mixing properties (Fry, 2002) (Fig. 4). We
248 used the most upstream and downstream samples as end-members for each year. In both years, nitrate concentrations plot
249 below the mixing line in the most upstream region with low salinity in both years, corresponding to an enrichment of $\delta^{15}\text{N-NO}_3^-$
250 and $\delta^{18}\text{O-NO}_3^-$ in the same region. Above a salinity of 20, a slight nitrate source is present, while isotope values decrease. In
251 2020, the outermost samples have a slightly enriched isotope signature and nitrate concentration below the mixing line.



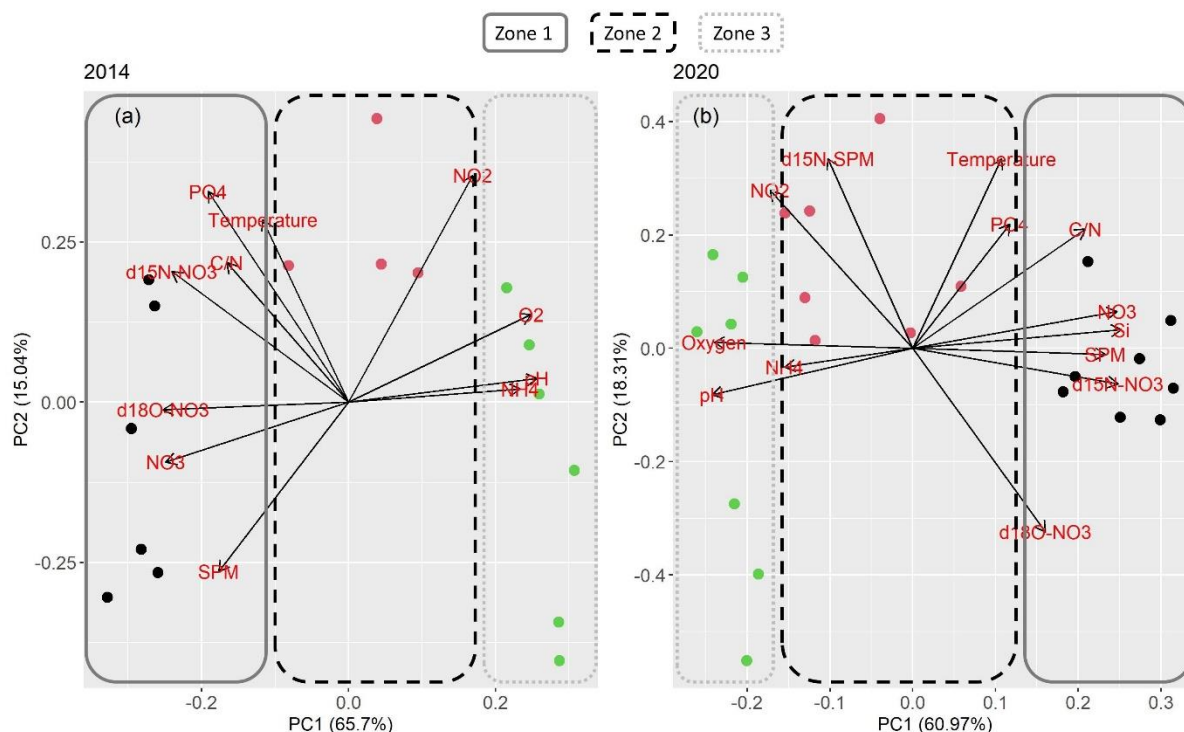
252

253 **Figure 4: Nitrate concentrations and isotope values of nitrate plotted versus salinity for (a), (b), (c) in 2014 and (d), (e), (f) in 2020.**
254 **Lines indicate calculated conservative mixing.**

255 3.5 Principal component analysis

256 Together, PC1 and PC2 explained about 80 % of total variance in both years. In 2014, PC1 contributed to 66 % and PC2 to
257 15 %. PC1 and PC2 explained 61 % and 18 % of total variance in 2020, respectively.

258 Oxygen, pH, C/N ratios, SPM and nitrate concentration contributed largely to PC1 in 2014, just like silicate concentration in
259 2020 (parameter were not measured in 2014). Temperature, phosphate and nitrite concentration contributed largely to PC2 in
260 both years, so did $\delta^{15}\text{N}$ -SPM in 2020. Due to few data, $\delta^{15}\text{N}$ -SPM could not be included into the principle component analysis
261 of 2014. In 2014, PC2 was also heavily influenced by SPM. The PCA overall suggests that the estuary can be divided into
262 three biogeochemically distinct zones, with zone 1 – “Tidal River”, zone 2 – “Dollard Reach/Middle Reaches”, and zone 3 –
263 “Outer Reaches” (Fig. 5).



264

265 **Figure 5: PCA results for (a) 2014 and (b) 2020. Point colors and frames stand for the assignment of the samples into the respective**
266 **zones. Dark blue points and a straight frame shows samples in zone 1 / Tidal River, red points and a dashed frame samples from**
267 **zone 2 / Dollard Reach and Middle Reaches. Green points and a dotted frame stand for samples in zone 3 / Outer Reaches.**

268 4 Discussion

269 4.1 Biogeochemical zones in the Ems Estuary

270 The first goal of this study was to identify distinct zones of nitrogen turnover within the Ems estuary to see if changing
271 environmental and geomorphological properties affect the occurring processes. The assessment of estuarine mixing curves
272 showed three zones of different nitrogen turnover along the salinity gradient (Fig. 4).

273 In both years, 2014 and 2020, nitrate concentration deviated clearly and in a similar manner from the conservative mixing line.
274 In the upper riverine part of the estuary, nitrate concentration fell below the conservative mixing line, indicating nitrate removal
275 (zone 1), followed by a zone with nitrate concentration slightly above the mixing line (zone 2) that acted as a net nitrate source.
276 In the third zone, nitrate mostly followed the conservative mixing line, with nitrate removal and isotopic enrichment near the
277 marine endmember in 2020, indicating nitrate uptake by phytoplankton.

278 The PCA support the suggested nitrate zonation taking the other biogeochemical properties into account (Fig. 5). The three
279 zones were mainly divided according to PC1. Contributing parameters were oxygen, nitrate, C/N, SPM and silicate, which



280 suggests a tight coupling of nitrate turnover to suspended particulate matter. PC2 helped to differentiate zone 2. Contributing
281 parameters (temperature, nitrite, and phosphate) suggest a link to nutrient uptake processes.
282 Based on the location of zones along the Ems (Fig. 1), we see a connection with the geomorphological characteristics of the
283 Ems estuary. In both years, zone 1 was located in the hyper-turbid Tidal River and the beginning of zone 2 is characterized by
284 increasing ammonium concentration. In 2014, zone 1 included the Dollard Reach. In 2020, the Dollard Reach was grouped
285 into zone 2, together with the Middle Reaches. The shift of zone 2 between the cruises may be driven by discharge conditions:
286 In 2014, discharge was significantly higher than 2020 (about twice the long-term average discharge of 30 to 40 m³ s⁻¹ for June
287 and August) (NLWKN Bst. Aurich and Engels, 2021), which may have led to a shift of zone 2 downstream as also indicated
288 by the shift in the salinity gradient and SPM concentrations. De Jonge et al. (2014) showed that elevated discharge can relocate
289 estuarine turbidity maxima downstream. Zone 3 was in the Outer Reaches in 2014 and 2020.
290 Overall, mixing properties as well as a PCA suggest that there are three distinct biogeochemical zones that act either as sinks
291 (zone 1 and 3) or sources (zone 2) of nitrate along the Ems. These ones are mainly defined by discharge and suspended
292 particulate matter (especially PC1).

293 **4.2 Denitrification in the upper estuary**

294 Zone 1, the most upstream region acted as a nitrate sink in both years, with nitrate concentrations below the conservative
295 mixing line and enriched $\delta^{15}\text{N-NO}_3^-$ and $\delta^{18}\text{O-NO}_3^-$ values (Fig. 4d and 4e). Potential removal mechanisms are nitrate
296 respiration or nitrate assimilation.
297 High SPM values in the hyper-turbid Tidal River and Dollard Reach (Fig. 2i) reduced light availability, limiting primary
298 production (Bos et al., 2012). Therefore, phytoplankton assimilation in the upper estuary can be ruled out as a relevant nitrate
299 sink.
300 Denitrification is a potential nitrate sink that can lead to strong isotope enrichment. Denitrification was a dominant loss pathway
301 in the 1980s in other temperate estuaries like the Elbe Estuary (Schróder et al., 1995), where sediment denitrification removed
302 up to 40 % of the summer nitrate load. We found that $\delta^{15}\text{N-NO}_3^-$ and $\delta^{18}\text{O-NO}_3^-$ in the Ems estuary increased with decreasing
303 nitrate concentration. $\delta^{15}\text{N-NO}_3^-$ versus $\delta^{18}\text{O-NO}_3^-$ plot on a slope of 0.5 in both years, which points towards denitrification
304 (Supplement Material S2) (Böttcher et al., 1990; Mengis et al., 1999; Granger and Wankel, 2016; Wong et al., 2020). A strong
305 fractionation occurred ($^{15}\epsilon \sim 24 \text{ ‰}$, $R^2 = 0.89$ in 2014 and 26 ‰ , $R^2 = 0.76$ in 2020). While denitrification in sediments leads
306 to little to no fractionation due to a diffusion limitation (Brandes and Devol, 1997; Lehmann et al., 2004; Sigman and Fripiat,
307 2018), water column denitrification has an isotope effect that fits our calculations (Kendall et al., 2007; Sigman and Fripiat,
308 2018), and can explain the observed patterns.
309 Water column denitrification occurs under anaerobic to low oxygen conditions in the water column (Tiedje, 1988). According
310 to Seitzinger (1988), denitrification occurs at oxygen concentration below 6.25 μM . We measured low oxygen concentration
311 in surface water during both years with lowest concentration of $\sim 70 \mu\text{mol L}^{-1}$ (Fig. 2h), which is well above the threshold for
312 denitrification. However, vertical oxygen concentration profiles and continuous measurements in the estuary in near-bottom



313 water showed that deeper water became anoxic in both years. Even though these anoxic conditions only developed for a few
314 hours over a tidal cycle, we conclude that water column denitrification was the responsible nitrate sink mechanism in the Ems
315 in 2014 and 2020.

316 Furthermore, denitrification can also occur on suspended particles. Liu et al. (2013) reported the occurrence of denitrification
317 on suspended particles in oxic waters in a hyper-turbid river. Xia et al. (2016) observed a high oxygen influx around suspended
318 particles and decreasing oxygen concentration. They suggest that oxygen was consumed by nitrification and/or microbial
319 respiration close to the particle's surface and thereby provided redox conditions for coupled nitrification-denitrification to take
320 place. Zhu et al. (2018) detected aggregates of nitrifiers and denitrifiers on SPM in the Hangzhou Bay in China. Similarly,
321 Sanders and Laanbroek (2018) propose that coupled nitrification-denitrification processes occur in the upper Ems estuary, and
322 suggested immediate nitrate consumption driven by suspended particles in the water column.

323 Overall, we find strong evidence for water column denitrification as in the Tidal River / zone 1, likely in the anoxic bottom
324 waters. Moreover, coupled nitrification-denitrification can add to this nitrate sink in the hyper-turbid Tidal River.

325 **4.3 Increasing importance of nitrification in the Middle Reaches**

326 The mixing lines along the estuary displayed a significant shift of nitrogen turnover from the zone 1 (Tidal River) to zone 2
327 (Dollard Reach/Middle Reaches). Nitrate concentration plotted above the mixing line, indicating a net nitrate source with
328 lighter nitrate isotope values (Fig. 4).

329 Nitrate is produced via nitrification, which was no longer oxygen limited in zone 2 due to increasing concentrations compared
330 to the Tidal River. A positive correlation between nitrite and ammonium, as well as a negative correlation between nitrite and
331 nitrate for both years indicate nitrate production via nitrification with nitrite as an intermediate product. This is in line with the
332 findings of Sanders and Laanbroek (2018), who found nitrification in water column and sediments in 2014.

333 However, there is no clear indication of nitrification in the correlations of nitrate concentration and nitrate isotopes. Nitrate
334 isotopes were positively correlated with nitrate concentrations, but such a parallel increase usually does not occur during
335 nitrification. Nitrification produces isotopically depleted nitrate, but the source of $\delta^{15}\text{N-NO}_3^-$ and $\delta^{18}\text{O-NO}_3^-$ are independent
336 and it increases the overall nitrate pool. At least in 2014, a plot of $\delta^{15}\text{N-NO}_3^-$ versus $\delta^{18}\text{O-NO}_3^-$ still plots on a slope of 0.5 in
337 2014, suggesting that denitrification may still be of importance in this zone. During denitrification, nitrate isotope values and
338 concentration are also negatively correlated, because denitrification consumes light nitrate and elevates the isotope values in
339 the remaining pool.

340 The positive correlation in our study thus is intriguing. It seems likely that denitrification still occurs in parts of zone 2, either
341 in the oxygen limited conditions in deeper water layers, in the sediments of the adjacent tidal flats (compare to Gao et al.,
342 2010) or driven by still elevated SPM concentrations of 185 and 230 mg L^{-1} in 2014 and 2020 respectively. The net addition
343 of nitrate, however, is a clear sign of nitrification.

344 Accordingly, we aim to explore whether the parallel increase of nitrate concentration and isotope values can be explained by
345 simultaneous nitrification and denitrification. To identify the influence of both processes, we used a mapping approach inspired



346 by Lewicka-Szczebak et al. (2017). A detailed description of the open-system mapping approach and figures are shown in the
347 supplementary material (S2). Briefly, we try to disentangle the influence of nitrification and denitrification in zone 2 based on
348 the open-system isotope effects, where the slope of the linear relationship between nitrate isotope values and remaining fraction
349 of nitrate concentration corresponds to the isotope effect (Sigman et al., 2009). The initial values used for the mapping are
350 derived from the nitrate mixing calculations based on Fry (2002).

351 For denitrification, we calculated an isotope effect of $^{15}\epsilon_{\text{DENIT}} = -26 \text{ ‰}$ in zone 1. For nitrification, the expression of the isotope
352 effect depends on the abundance of ammonium. As long as ammonium is limiting, we assume that any ammonium is converted
353 to nitrite and nitrate, so that the apparent isotope effect is that of remineralisation, as long as ammonium concentration is low.
354 In most parts 2, no ammonium was accumulated. A simultaneous increase of $\delta^{15}\text{N-SPM}$, ammonium and nitrite concentration
355 at stream kilometer 50 in 2020 point towards remineralisation (Fig. 2a, 2b and 2l). Based on $\delta^{15}\text{N-SPM}$, we calculated an
356 isotope effect of $^{15}\epsilon_{\text{REMIN}} = -1.2 \text{ ‰}$ ($R^2 = 0.26$), which fits with previous assessments of the isotope effect of ammonification
357 (Möbius, 2013). We applied this value for nitrification with prior remineralisation. Further downstream, ammonium and nitrite
358 concentrations increased, so that we assume that remineralisation no longer determines the overall isotope effect of
359 nitrification. Instead, there was a combined influence of ammonium oxidation with an isotope effect $^{15}\epsilon = -14$ to -41 ‰
360 (Mariotti et al., 1981; Casciotti et al., 2003; Santoro and Casciotti, 2011) and nitrite oxidation with $^{15}\epsilon = +9$ to $+20 \text{ ‰}$ (Casciotti,
361 2009; Buchwald and Casciotti, 2010; Jacob et al., 2017). As we measured elevated ammonium and nitrite concentrations, both
362 processes influenced the fractionation caused by nitrification. Therefore, for total nitrification we assumed a combined isotope
363 effect of $^{15}\epsilon_{\text{NITRI}} = -10 \text{ ‰}$, that we used to describe nitrification in samples with accumulated ammonium and nitrite. This
364 number is lower than previously measured for ammonium oxidation, and is based on nitrification rate from incubations
365 performed previously in the Elbe estuary (Sanders, unpublished data).

366 Based on these input variables, the mapping approach can indeed explain the development of isotope effects and nitrate
367 concentration. In the most upstream samples, nitrate removal exceeded production: In 2014, denitrification removed
368 $26 \mu\text{mol L}^{-1}$, and nitrification added $10 \mu\text{mol L}^{-1}$. In 2020, the mapping approach suggests an addition of $52 \mu\text{mol L}^{-1}$ and
369 simultaneous denitrification of $62 \mu\text{mol L}^{-1}$. In the middle of zone 2 nitrification gained in relative importance with an
370 approximated production of $10 \mu\text{mol L}^{-1}$ in 2014 and $20 \mu\text{mol L}^{-1}$ in 2020, in contrast to denitrification of approximately
371 $3 \mu\text{mol L}^{-1}$ and $10 \mu\text{mol L}^{-1}$ respectively. In the most downstream samples, mixing was dominant, and we detected neither
372 nitrate production nor reduction.

373 Overall, nitrification and denitrification determined the evolution of nitrate isotopes and concentration in the estuary.
374 Downstream zone 2, nitrification becomes increasingly important, and the relevance of denitrification ceases. Both processes
375 lose in importance towards the North Sea, when mixing turns to be the most important process.

376 4.4 Mixing and nitrate uptake in the Outer Reaches

377 In the Outer Reaches/zone 3 the mixing line shows divergent trends for our two cruises (Fig. 4). While conservative mixing
378 dominates in 2014, 2020 shows nitrate uptake in the North Sea.



379 For 2020, a plot of $\delta^{15}\text{N-NO}_3^-$ versus $\delta^{18}\text{O-NO}_3^-$ falls along a slope of 1.5, which points towards simultaneous assimilation and
380 nitrification (Wankel et al., 2006; Dähnke et al., 2010). The isotope effect $^{15}\epsilon$ of this drawdown is - 3 ‰, which also is a sign
381 for assimilation, even though it is at the lower end of values reported for pure cultures (Granger et al., 2004). C/N values close
382 to Redfield Ratio in 2020 (Fig. 2j) also pointed towards primary production in the Outer Reaches. The stronger signal of nitrate
383 uptake in June 2020 compared to August 2014 is likely caused by a stronger influence of the spring phytoplankton bloom in
384 the Outer Reaches (Colijn, 1983; Colijn et al., 1987; Brinkman et al., 2015) fueled by continuous nutrient supply from the
385 estuary.

386 In the mixing plot (Fig. 4), the outermost isotope samples of our cruise in 2020 fall on the conservative mixing line. The good
387 fit is caused by the calculation with a marine endmember that has an isotopically enriched signature in comparison to average
388 global values (Sigman et al., 2000, 2009) and North Sea winter values of 5 ‰ (Dähnke et al., 2010). The increase of the isotope
389 signature shows that fractionation takes place, likely due to assimilation.

390 In contrast to the biogeochemical active inner zones, mixing dominated nitrate distribution in the Outer Reaches of the estuary
391 in 2014. In 2020 however, the Outer Reaches were a nitrate sink due to ongoing primary production in the coastal North Sea.

392 **4.5 SPM as driving force of the spatial zonation**

393 We identified three zones of nitrogen turnover along the estuary, which differ significantly in their coastal filter function. The
394 Tidal River was a nitrate sink with dominating water column denitrification. In the Middle Reaches, nitrification gained in
395 importance, turning this section in a net nitrate source. In the Outer Reaches / zone 3, mixing gained in importance but with a
396 clear nutrient uptake in 2020. Other estuaries with high turbidity show strong denitrification zones as well (Ogilvie et al., 1997;
397 Middelburg and Nieuwenhuize, 2001). This finding and our analysis of the PCA and dominant nitrogen turnover processes
398 suggest that the overarching control on biogeochemical nitrogen cycling and zonation may be suspended particulate matter.

399 Channel deepening led to tidal amplification and an increased sediment transport in the estuary (Winterwerp et al., 2013; De
400 Jonge et al., 2014; Van Maren et al., 2015b, a). Between 1954 and 2005, SPM concentration increased on average 2- to 3-fold,
401 and even 10-fold in the Tidal River. The turbidity maximum extended to a length of 30 km and moved upstream, into the
402 freshwater Tidal River (De Jonge et al., 2014).

403 High C/N ratios (Fig. 2j), as well as a low and stable particular organic carbon (POC) fraction of the SPM in this region (~
404 4.5 %) in the Tidal River and Dollard Reach indicate low organic matter quality and a large contribution of mineral associated
405 organic matter of the present organic matter (Fig. 2k). In 2014, C/N ratios were extremely high, and uncharacteristic for
406 estuarine environments. We attribute this to a potential influence of peat soils or peat debris in sediments (Broder et al., 2012;
407 Loisel et al., 2012; Wang et al., 2015; Papenmeier et al., 2013), which may have been washed into the river due to high
408 discharge. The extremely high C/N ratios should nonetheless be treated with caution, as we cannot entirely rule out sampling
409 artifacts.



410 Nonetheless, and regardless of organic matter origin, degradation of organic carbon leads to anoxic conditions in the Tidal
411 River. Even though the low quality of organic matter fuels only low degradation rates with POC fractions of ~ 3 % (Fig. 2k),
412 the extremely high POC concentration ($> 4000 \mu\text{mol L}^{-1}$) support the intense oxygen depletion and anoxic conditions in the
413 Tidal River. This indicates very refractory material. Talke et al. (2009) found oxygen depletion rates proportional to SPM
414 concentrations in the Ems estuary. Moreover, high SPM concentrations depress primary production throughout the inner
415 estuary due to light limitation and leads to a dominance of heterotrophic processes (Bos et al., 2012).

416 With decreasing SPM concentration, oxygen concentration increases, and the relevance of denitrification ceases in comparison
417 to nitrification. In zone 2 at the transition between Dollard Reach and Middle Reaches, C/N ratios start to decrease, indicating
418 the input of fresh organic matter entering the estuary from the North Sea (Van Beusekom and de Jonge, 1997, 1998) fueling
419 nitrification in zone 2. Although, the quality of the organic matter improves, oxygen depletion decreases due to reduced SPM
420 concentrations leading to lower POC concentrations in comparison to the Tidal River. Towards the North Sea, low SPM
421 concentration in the Outer Reaches enable deeper light penetrations supporting local primary production (Liu et al., 2018;
422 Colijn et al., 1987) as also supported by a slight chlorophyll maximum in the Outer Reaches (S4). Given the ongoing import
423 of organic matter from the North Sea to the Wadden Sea and adjacent estuaries, this primary produced organic material
424 probably fuels the remineralisation process in the inner estuary.

425 Changing discharge conditions can lead to a spatial shift of zones within the estuary. De Jonge et al. (2014) already showed
426 that elevated discharge relocate ETM in downstream position. As we identified SPM concentration as one of the most important
427 controls on nitrogen turnover in the Ems estuary, we assume that the zones will move with shifting SPM concentration along
428 the estuary.

429 Overall, we find that the interplay of nitrification/denitrification and assimilation is governed by SPM concentration along the
430 Ems estuary. We expect that changing discharge can lead to spatial offsets in SPM concentrations and thus influence the spatial
431 segregation nitrogen turnover processes.

432 **4.6 Nitrous oxide production and its controls in the Ems estuary**

433 So far, we elucidated nitrogen turnover in the Ems Estuary. We found that nitrification and denitrification vary spatially in
434 importance. Both processes can produce nitrous oxide, and we accordingly found nitrous oxide peaks in the estuary in areas
435 with significant differences in their nitrogen turnover. Nitrous oxide was measured only in 2020, thus we will use the high-
436 resolution data from this cruise to examine the importance nitrification and denitrification for nitrous oxide production along
437 the estuary. We will also discuss controls that favor the emergence of nitrous oxide production areas.

438 The calculated average sea-to-air flux of $0.35 \text{ g-N}_2\text{O m}^{-2} \text{ a}^{-1}$ results in a total nitrous oxide emission of $0.57 \times 10^8 \text{ g-N}_2\text{O a}^{-1}$
439 along the Ems estuary. In June 1997, a significantly higher average sea-to-air flux density of $1.23 \text{ g-N}_2\text{O m}^{-2} \text{ a}^{-1}$ was measured
440 (Barnes and Upstill-Goddard, 2011), which amounted to an annual nitrous oxide emission of $2.0 \times 10^8 \text{ g-N}_2\text{O a}^{-1}$ over the



441 entire estuary. Upscaling from a single cruise to an entire year is somewhat questionable, but it interesting to note that the
442 emissions may have halved since the 1990s. Furthermore, our results as well as those from 1997 were obtained from a single
443 survey in June making the comparison intriguing. Since the 1990s, the DIN load of the Ems estuary was significantly reduced
444 due to management efforts (Bos et al., 2012). Phytoplankton biomass in the Outer Reaches (Station Huibertgat Oost, Van
445 Beusekom et al., 2018) decreased in response to decreasing nutrient loads, possibly contributing to the observed lower N₂O
446 emissions. However, this hypothesis requires verification in the future.

447 The nitrous oxide concentrations observed in 2020 can be linked to the prevailing biogeochemical conditions. The first nitrous
448 oxide maximum was located in the upstream region (stream kilometer 0). In this area, we identified water column
449 denitrification as the dominant nitrogen turnover process, and we found relatively low pH values and high nitrate concentration.
450 In their summary paper about nitrous oxide in streams and rivers, Quick et al. (2019) found that these factors are favorable for
451 nitrous oxide production via denitrification. Intermittent oxygen hypoxia and anoxia in the different water depths also enhance
452 nitrous oxide production in the Tidal River, which is in line with our tidal oxygen measurements in the Ems. Several studies
453 also showed a positive correlation between nitrous oxide concentration and SPM concentration (Tiedje, 1988; Liu et al., 2013;
454 Zhou et al., 2019), and SPM concentration was also highest in this region of the Tidal River. Altogether, we suggest that the
455 Ems is well suited as a region with extremely high nitrous oxide production, triggered by high nutrient loss, intermittent anoxia,
456 and high SPM loads.

457 Further downstream, nitrous oxide concentrations decrease, along with oxygen concentrations, reaching a minimum around
458 km 22. The simultaneous reduction of nitrous oxide and oxygen concentration at first sight seems counterintuitive, but it may
459 be caused by complete denitrification that produces N₂ instead of nitrous oxide (Knowles, 1982).

460 Based on our data, we cannot clearly say whether the source of nitrous oxide production was in the water column or in
461 sediments. Other studies, e.g. in the muddy Colne estuary found high nitrous oxide production due to denitrification, but
462 assigned nitrous oxide production only to the sediments (Ogilvie et al., 1997; Robinson et al., 1998; Dong et al., 2002).
463 Sedimentary denitrification in our study may have contributed to this first nitrous oxide maximum. The beginning of ebb tide
464 during our campaign may have enhanced outgassing of nitrous oxide from the sediment, and low water levels may have caused
465 a mechanical release of nitrous oxide from the sediments caused by our research vessel. Thus, zone 1 is an important nitrous
466 oxide production zone, but the measured nitrous oxide concentration might in parts be affected by sedimentary processes and
467 might overestimates nitrous oxide production in the water column.

468 The second nitrous oxide maximum occurred around stream kilometer 35 at the transition between Tidal River and Dollard
469 Reach. In this area, our mapping approach indicates simultaneous denitrification and nitrification. The nitrous oxide peak
470 coincides with an increase of ammonium and nitrite concentration as well as a slight rise in nitrate concentration, indicating
471 the onset of nitrification in the water column.



472 In contrast to condition leading to the first nitrous oxide peak, not enough fresh organic matter seems to be present in the
473 transition area to support nitrous oxide production. Lower SPM concentrations with comparable low POC fraction leads to
474 lower remineralisation rates and higher oxygen levels. Low organic matter availability and increasing oxygen concentration
475 favor nitrous oxide production via nitrification (Otte et al., 1999; Sutka et al., 2006). Similarly, Quick et al. (2019) summarized
476 aerobic or oxygen limited conditions with low organic carbon availability favorable for nitrous oxide production via
477 nitrification. As our data suggests additional denitrification, we speculate that in possible anoxic microsites on suspended
478 particles and anoxic deeper water layers, denitrification may have contributed to nitrous oxide production. Overall, we assume
479 that nitrification and denitrification jointly added to nitrous oxide production in this region.

480 In summary, we find that two nitrous oxide production hotspots exist in the Ems estuary. SPM plays a big role controlling the
481 nitrous oxide production along the Ems estuary. In the upstream region, where oxygen depletion occurs due to immense SPM
482 concentration, denitrification produces nitrous oxide. At the transition zone between Tidal River and Dollard Reach, SPM
483 concentration is lower, leading to higher oxygen concentration and nitrous oxide production via nitrification. Denitrification
484 prevails in deeper water layers where oxygen concentration is low, and possibly in anoxic microsites close to particles.

485 **Conclusion**

486 Overall, the Ems estuary acted as a nitrate sink in both years. However, we found that three distinct biogeochemical zones
487 exist along the Ems. Stable isotope changes point towards water column denitrification in the turbid water column of the Tidal
488 River. In the Dollard Reach/Middle Reaches nitrification gains importance turning this section of the estuary into a net nitrate
489 source. Nitrate uptake occurs in the Outer Reaches due to primary production in the coastal North Sea, in August 2014 mixing
490 dominated. Our analysis of the dominant nitrogen turnover processes suggest that SPM concentration and the linked oxygen
491 deficits exert the overarching control on biogeochemical nitrogen cycling, zonation and nitrous oxide production in the Ems
492 estuary.

493 Changing biogeochemical conditions can significantly alter estuarine nutrient processing. Deepening of rivers happens not
494 only in Germany (Kerner, 2007; Schuchardt and Scholle, 2009; De Jonge et al., 2014; Van Maren et al., 2015b) but worldwide
495 (e.g. Van Maren et al. 2009; Winterwerp et al. 2013; Cox et al. 2019; Grasso and Le Hir 2019; Pareja-Roman et al. 2020), and
496 this can change SPM loads and composition in estuaries. Increased SPM loads can enhance denitrification, but also trigger
497 nitrous oxide production and enhance oxygen-depleted zones. Thus, the interplay of SPM with riverine nutrient filter function
498 and nitrous oxide emissions should be evaluated. The common practices of deepening and dredging affect SPM and this pose
499 a direct link between pressing social and ecological problems in coastal areas.



500 **Data availability**

501 Data will be available under coastMap Geoportail (www.coastmap.org) connecting to PANGAEA. (<https://www.pangaea.de/>)
502 with DOI availability.

503 **Author contribution**

504 GS, TS and KD designed this study. GS did the sampling, sample measurement and analyses for the cruise of 2020 as well as
505 the data interpretation and evaluation. TS did the sampling and sample measurement for the cruise in 2014. YV provided the
506 oxygen data and correction from the FerryBox. AS provided the oxygen data from German Federal Institute of Hydrology.
507 KD, AS, YS, JB and TS contributed with scientific and editorial recommendations. GS prepared the manuscript with
508 contributions from all co-authors.

509 **Competing interest**

510 The authors declare that they have no conflict of interest.

511 **Acknowledgment and Funding**

512 This study was funded by the Deutsche Forschungsgemeinschaft (DFG, German Research Foundation) under Germany's
513 Excellence Strategy – EXC 2037 'CLICCS - Climate, Climatic Change, and Society' – Project Number: 390683824,
514 contribution to the Center for Earth System Research and Sustainability (CEN) of Universität Hamburg.

515 We thank the crew of R/V Ludwig Prandtl for the great support during the cruises. Thanks to Leon Schmidt, who measured
516 the nutrients and helped during the field work. Phillip Wiese is gratefully acknowledge for the isotope analyses of the 2014
517 sampling. We are thankful for the FerryBox Team: Martina Gehrung for the preparation and Tanja Pieplow for the oxygen
518 measurements. Thanks to the working group of Biogeochemistry at the Institute for Geology for measuring C/N ratios, POC
519 fractions and $\delta^{15}\text{N}$ -SPM values.

520

521 **References**

522 Bange, H. W.: Nitrous oxide and methane in European coastal waters, *Estuar. Coast. Shelf Sci.*, 70, 361–374,
523 <https://doi.org/10.1016/j.ecss.2006.05.042>, 2006.

524 Barnes, J. and Upstill-Goddard, R. C.: N₂O seasonal distributions and air-sea exchange in UK estuaries: Implications for the
525 tropospheric N₂O source from European coastal waters, *J. Geophys. Res. Biogeosciences*, 116,
526 <https://doi.org/10.1029/2009JG001156>, 2011.



- 527 Billen, G., Silvestre, M., Grizzetti, B., Leip, A., Garnier, J., Voss, M., Howarth, R., Bouraoui, F., Lepistö, A., Kortelainen, P.,
528 Johnes, P., Barford, C., Humborg, C., Smedberg, E., Kaste, Ø., Ganeshram, R., Beusen, A., and Lancelot, C.: Nitrogen flows
529 from European regional watersheds to coastal marine waters, in: *The European Nitrogen Assessment: Sources, Effects and*
530 *Policy Perspectives*, Cambridge University Press, 271–297, 2011.
- 531 Borges, A., Vanderborght, J.-P., Schiettecatte, L.-S., Gazeau, F., Ferrón-Smith, S., Delille, B., and Frankignoulle, M.:
532 Variability of gas transfer velocity of CO₂ in a macrotidal estuary (The Scheldt), *Estuaries*, 27, 593–603,
533 <https://doi.org/10.1007/BF02907647>, 2004.
- 534 Bos, D., Büttger, H., Esselink, P., Jager, Z., de Jonge, V. N., Kruckenberg, H., van Maren, D. S., and Schuchardt, B.: *The*
535 *ecological state of the Ems estuary and options for restoration*, 2012.
- 536 Böttcher, J., Strelbel, O., Voerkelius, S., and Schmidt, H.-L.: Using isotope fractionation of nitrate-nitrogen and nitrate-oxygen
537 for evaluation of microbial denitrification in a sandy aquifer, *J. Hydrol.*, 114, 413–424, [https://doi.org/10.1016/0022-](https://doi.org/10.1016/0022-1694(90)90068-9)
538 [1694\(90\)90068-9](https://doi.org/10.1016/0022-1694(90)90068-9), 1990.
- 539 Bouwman, A. F., Bierkens, M. F. P., Griffioen, J., Hefting, M. M., Middelburg, J. J., Middelkoop, H., and Slomp, C. P.:
540 Nutrient dynamics, transfer and retention along the aquatic continuum from land to ocean: towards integration of ecological
541 and biogeochemical models, *Biogeosciences*, 10, 1–22, <https://doi.org/10.5194/bg-10-1-2013>, 2013.
- 542 Brandes, J. A. and Devol, A. H.: Isotopic fractionation of oxygen and nitrogen in coastal marine sediments, *Geochim.*
543 *Cosmochim. Acta*, 61, 1793–1801, [https://doi.org/10.1016/S0016-7037\(97\)00041-0](https://doi.org/10.1016/S0016-7037(97)00041-0), 1997.
- 544 Brase, L., Bange, H. W., Lendt, R., Sanders, T., and Dähnke, K.: High Resolution Measurements of Nitrous Oxide (N₂O) in
545 the Elbe Estuary, *Front. Mar. Sci.*, 4, 162, <https://doi.org/10.3389/fmars.2017.00162>, 2017.
- 546 Brinkman, A. G., Riegman, R., Jacobs, P., Kuhn, S., and Meijboom, A.: *Ems-Dollard primary production research: Full data*
547 *report*, Institute for Marine Resources & Ecosystem Studies, 2015.
- 548 Broder, T., Blodau, C., Biester, H., and Knorr, K. H.: Peat decomposition records in three pristine ombrotrophic bogs in
549 southern Patagonia, *Biogeosciences*, 9, 1479–1491, <https://doi.org/10.5194/bg-9-1479-2012>, 2012.
- 550 Buchwald, C. and Casciotti, K. L.: Oxygen isotopic fractionation and exchange during bacterial nitrite oxidation, *Limnol.*
551 *Oceanogr.*, 55, 1064–1074, <https://doi.org/10.4319/lo.2010.55.3.1064>, 2010.
- 552 Carstensen, J., Conley, D. J., Bonsdorff, E., Gustafsson, B. G., Hietanen, S., Janas, U., Jilbert, T., Maximov, A., Norkko, A.,
553 Norkko, J., Reed, D. C., Slomp, C. P., Timmermann, K., and Voss, M.: Hypoxia in the Baltic Sea: biogeochemical cycles,
554 benthic fauna, and management, *Ambio*, 43, 26–36, <https://doi.org/10.1007/s13280-013-0474-7>, 2014.
- 555 Casciotti, K. L.: Inverse kinetic isotope fractionation during bacterial nitrite oxidation, *Geochim. Cosmochim. Acta*, 73, 2061–
556 2076, <https://doi.org/10.1016/j.gca.2008.12.022>, 2009.
- 557 Casciotti, K. L., Sigman, D. M., Hastings, M. G., Böhlke, J. K., and Hilkert, A.: Measurement of the Oxygen Isotopic
558 Composition of Nitrate in Seawater and Freshwater Using the Denitrifier Method, *Anal. Chem.*, 74, 4905–4912,
559 <https://doi.org/10.1021/ac020113w>, 2002.
- 560 Casciotti, K. L., Sigman, D. M., and Ward, B. B.: Linking Diversity and Stable Isotope Fractionation in Ammonia-Oxidizing
561 Bacteria, *Geomicrobiol. J.*, 20, 335–353, <https://doi.org/10.1080/01490450303895>, 2003.
- 562 Colijn, F.: *Primary production in the Ems Dollard estuary*, State University Groningen, Groningen, 1983.



- 563 Colijn, F., Admiraal, W., Baretta, J. W., and Ruardij, P.: Primary production in a turbid estuary, the Ems-Dollard: field and
564 model studies, *Cont. Shelf Res.*, 7, 1405–1409, [https://doi.org/10.1016/0278-4343\(87\)90045-8](https://doi.org/10.1016/0278-4343(87)90045-8), 1987.
- 565 Compton, T. J., Holthuijsen, S., Mulder, M., van Arkel, M., Schaars, L. K., Koolhaas, A., Dekinga, A., ten Horn, J.,
566 Luttkhuizen, P. C., van der Meer, J., Piersma, T., and van der Veer, H. W.: Shifting baselines in the Ems Dollard estuary: A
567 comparison across three decades reveals changing benthic communities, *J. Sea Res.*, 127, 119–132,
568 <https://doi.org/10.1016/j.seares.2017.06.014>, 2017.
- 569 Cox, T. J. S., Maris, T., Van Engeland, T., Soetaert, K., and Meire, P.: Critical transitions in suspended sediment dynamics in
570 a temperate meso-tidal estuary, *Sci. Rep.*, 9, 12745, <https://doi.org/10.1038/s41598-019-48978-5>, 2019.
- 571 Crossland, C. J., Baird, D., Ducrottoy, J.-P., Lindeboom, H., Buddemeier, R. W., Dennison, W. C., Maxwell, B. A., Smith, S.
572 V., and Swaney, D. P.: The Coastal Zone — a Domain of Global Interactions, in: *Coastal Fluxes in the Anthropocene: The*
573 *Land-Ocean Interactions in the Coastal Zone Project of the International Geosphere-Biosphere Programme*, edited by:
574 Crossland, C. J., Kremer, H. H., Lindeboom, H. J., Marshall Crossland, J. I., and Le Tissier, M. D. A., Springer, Berlin,
575 Heidelberg, 1–37, https://doi.org/10.1007/3-540-27851-6_1, 2005.
- 576 Dähnke, K., Bahlmann, E., and Emeis, K.-C.: A nitrate sink in estuaries? An assessment by means of stable nitrate isotopes in
577 the Elbe estuary, *Limnol. Oceanogr.*, 53, 1504–1511, <https://doi.org/10.4319/lo.2008.53.4.1504>, 2008.
- 578 Dähnke, K., Emeis, K.-C., Johannsen, A., and Nagel, B.: Stable isotope composition and turnover of nitrate in the German
579 Bight, *Mar. Ecol. Prog. Ser.*, 408, 7–18, <https://doi.org/10.3354/meps08558>, 2010.
- 580 De Jonge, V. N.: Relations Between Annual Dredging Activities, Suspended Matter Concentrations, and the Development of
581 the Tidal Regime in the Ems Estuary, *Can. J. Fish. Aquat. Sci.*, 40, 289–300, <https://doi.org/10.1139/f83-290>, 1983.
- 582 De Jonge, V. N., Schuttelaars, H. M., van Beusekom, J. E. E., Talke, S. A., and de Swart, H. E.: The influence of channel
583 deepening on estuarine turbidity levels and dynamics, as exemplified by the Ems estuary, *Estuar. Coast. Shelf Sci.*, 139, 46–
584 59, <https://doi.org/10.1016/j.ecss.2013.12.030>, 2014.
- 585 Deutsch, B., Mewes, M., Liskow, I., and Voss, M.: Quantification of diffuse nitrate inputs into a small river system using
586 stable isotopes of oxygen and nitrogen in nitrate, *Org. Geochem.*, 37, 1333–1342, 2006.
- 587 Diaz, R. J. and Rosenberg, R.: Spreading Dead Zones and Consequences for Marine Ecosystems, *Science*, 321,
588 <https://doi.org/10.1126/science.1156401>, 2008.
- 589 Diaz, R. J., Rosenberg, R., and Sturdivant, K.: Hypoxia in estuaries and semi- enclosed seas, in: *Ocean deoxygenation :
590 everyone’s problem*, IUCN, 20, 2019.
- 591 Dong, L., Nedwell, D. B., Underwood, G. J. C., Thornton, D. C. O., and Rusmana, I.: Nitrous oxide formation in the Colne
592 estuary, England: the central role of nitrite., *Appl. Environ. Microbiol.*, 68, <https://doi.org/10.1128/aem.68.3.1240-1249.2002>,
593 2002.
- 594 Francis, C. A., Beman, J. M., and Kuypers, M. M. M.: New processes and players in the nitrogen cycle: the microbial ecology
595 of anaerobic and archaeal ammonia oxidation, *ISME J.*, <https://doi.org/10.1038/ismej.2007.8>, 2007.
- 596 Fry, B.: Conservative mixing of stable isotopes across estuarine salinity gradients: A conceptual framework for monitoring
597 watershed influences on downstream fisheries production, *Estuaries*, 25, 264–271, <https://doi.org/10.1007/BF02691313>, 2002.



- 598 Galloway, J. N., Aber, J. D., Erisman, J. W., Seitzinger, S. P., Howarth, R. W., Cowling, E. B., and Cosby, B. J.: The Nitrogen
599 Cascade, *BioScience*, 53, 341–356, [https://doi.org/10.1641/0006-3568\(2003\)053\[0341:TNC\]2.0.CO;2](https://doi.org/10.1641/0006-3568(2003)053[0341:TNC]2.0.CO;2), 2003.
- 600 Gao, H., Schreiber, F., Collins, G., Jensen, M. M., Kostka, J. E., Lavik, G., de Beer, D., Zhou, H.-Y., and Kuypers, M. M. M.:
601 Aerobic denitrification in permeable Wadden Sea sediments, *ISME J.*, 4, 417–426, <https://doi.org/10.1038/ismej.2009.127>,
602 2010.
- 603 Giblin, A., Tobias, C., Song, B., Weston, N., Banta, G., and Rivera-Monroy, V.: The Importance of Dissimilatory Nitrate
604 Reduction to Ammonium (DNRA) in the Nitrogen Cycle of Coastal Ecosystems, *Oceanography*, 26, 124–131,
605 <https://doi.org/10.5670/oceanog.2013.54>, 2013.
- 606 Granger, J. and Sigman, D. M.: Removal of nitrite with sulfamic acid for nitrate N and O isotope analysis with the denitrifier
607 method, *Rapid Commun. Mass Spectrom.*, 23, 3753–3762, <https://doi.org/10.1002/rcm.4307>, 2009.
- 608 Granger, J. and Wankel, S.: Isotopic overprinting of nitrification on denitrification as a ubiquitous and unifying feature of
609 environmental nitrogen cycling, *Proc. Natl. Acad. Sci.*, 113, <https://doi.org/10.1073/pnas.1601383113>, 2016.
- 610 Granger, J., Sigman, D. M., Needoba, J. A., and Harrison, P. J.: Coupled nitrogen and oxygen isotope fractionation of nitrate
611 during assimilation by cultures of marine phytoplankton, *Limnol. Oceanogr.*, 49, 1763–1773,
612 <https://doi.org/10.4319/lo.2004.49.5.1763>, 2004.
- 613 Grasso, F. and Le Hir, P.: Influence of morphological changes on suspended sediment dynamics in a macrotidal estuary:
614 diachronic analysis in the Seine Estuary (France) from 1960 to 2010, *Ocean Dyn.*, 69, 83–100, [https://doi.org/10.1007/s10236-](https://doi.org/10.1007/s10236-018-1233-x)
615 [018-1233-x](https://doi.org/10.1007/s10236-018-1233-x), 2019.
- 616 Hansen, H. P. and Koroleff, F.: Determination of nutrients, in: *Methods of Seawater Analysis*, John Wiley & Sons, Ltd, 159–
617 228, <https://doi.org/10.1002/9783527613984.ch10>, 2007.
- 618 Howarth, . W.: Coastal nitrogen pollution: A review of sources and trends globally and regionally, *Harmful Algae*, 8, 14–20,
619 <https://doi.org/10.1016/j.hal.2008.08.015>, 2008.
- 620 Howarth, R. W. and Marino, R.: Nitrogen as the limiting nutrient for eutrophication in coastal marine ecosystems: Evolving
621 views over three decades, *Limnol. Oceanogr.*, 51, 364–376, https://doi.org/10.4319/lo.2006.51.1_part_2.0364, 2006.
- 622 IPCC: *Climate Change 2007: The Physical Science Basis. Contribution of Working Group I to the Fourth Assessment Report*
623 *of the Intergovernmental Panel on Climate Change*, 2007.
- 624 Jacob, J., Nowka, B., Merten, V., Sanders, T., Spieck, E., and Dähnke, K.: Oxidation kinetics and inverse isotope effect of
625 marine nitrite-oxidizing isolates, *Aquat. Microb. Ecol.*, 80, 289–300, <https://doi.org/10.3354/ame01859>, 2017.
- 626 Johannsen, A., Dähnke, K., and Emeis, K.: Isotopic composition of nitrate in five German rivers discharging into the North
627 Sea, *Org. Geochem.*, 39, 1678–1689, <https://doi.org/10.1016/j.orggeochem.2008.03.004>, 2008.
- 628 Kendall, C., Elliott, E. M., and Wankel, S. D.: Tracing Anthropogenic Inputs of Nitrogen to Ecosystems, in: *Stable Isotopes*
629 *in Ecology and Environmental Science*, John Wiley & Sons, Ltd, 375–449, <https://doi.org/10.1002/9780470691854.ch12>,
630 2007.
- 631 Kerner, M.: Effects of deepening the Elbe Estuary on sediment regime and water quality, *Estuar. Coast. Shelf Sci.*, 75, 492–
632 500, <https://doi.org/10.1016/j.ecss.2007.05.033>, 2007.



- 633 Knowles, R.: Denitrification, *Microbiol. Rev.*, 46, 43–70, 1982.
- 634 Krebs, M. and Weilbeer, H.: Ems-Dollart Estuary, *Küste*, 74, 252–262, 2008.
- 635 Lehmann, M. F., Sigman, D. M., and Berelson, W. M.: Coupling the 15N/14N and 18O/16O of nitrate as a constraint on
636 benthic nitrogen cycling, *Mar. Chem.*, 88, 1–20, <https://doi.org/10.1016/j.marchem.2004.02.001>, 2004.
- 637 Lewicka-Szczebak, D., Augustin, J., Giesemann, A., and Well, R.: Quantifying N₂O reduction to N₂ based on N₂O
638 isotopocules – validation with independent methods (helium incubation and 15N gas flux method), *Biogeosciences*, 14, 711–
639 732, <https://doi.org/10.5194/bg-14-711-2017>, 2017.
- 640 Liss, P. S.: Conservative and non-conservative behavior of dissolved constituents during estuarine mixing, in: In J. D. Burton
641 and J. D. Liss [eds.], *Estuarine chemistry*, Academic Press, 93–130, 1976.
- 642 Liu, B., de Swart, H. E., and de Jonge, V. N.: Phytoplankton bloom dynamics in turbid, well-mixed estuaries: A model study,
643 *Estuar. Coast. Shelf Sci.*, 211, 137–151, <https://doi.org/10.1016/j.ecss.2018.01.010>, 2018.
- 644 Liu, T., Xia, X., Liu, S., Mou, X., and Qiu, Y.: Acceleration of denitrification in turbid rivers due to denitrification occurring
645 on suspended sediment in oxic waters, *Environ. Sci. Technol.*, 47, 4053–4061, <https://doi.org/10.1021/es304504m>, 2013.
- 646 Loisel, J., Gallego-Sala, A. V., and Yu, Z.: Global-scale pattern of peatland *Sphagnum* growth driven by photosynthetically
647 active radiation and growing season length, *Biogeosciences*, 9, 2737–2746, <https://doi.org/10.5194/bg-9-2737-2012>, 2012.
- 648 Mariotti, A., Germon, J. C., Hubert, P., Kaiser, P., Letolle, R., Tardieux, A., and Tardieux, P.: Experimental determination of
649 nitrogen kinetic isotope fractionation: some principles, illustrations for the denitrification and nitrification process, *Plant Soil*,
650 62, 413–430, 1981.
- 651 Mengis, M., Schif, S. L., Harris, M., English, M. C., Aravena, R., Elgood, R., and MacLean, A.: Multiple Geochemical and
652 Isotopic Approaches for Assessing Ground Water NO₃– Elimination in a Riparian Zone, *Groundwater*, 37, 448–457,
653 <https://doi.org/10.1111/j.1745-6584.1999.tb01124.x>, 1999.
- 654 Middelburg, J. and Nieuwenhuize, J.: Uptake of dissolved inorganic nitrogen in turbid, tidal estuaries, *Mar. Ecol.-Prog. Ser.*,
655 192, 79–88, <https://doi.org/10.3354/meps192079>, 2001.
- 656 Möbius, J.: Isotope fractionation during nitrogen remineralization (ammonification): Implications for nitrogen isotope
657 biogeochemistry, *Geochim. Cosmochim. Acta*, 105, 422–432, <https://doi.org/10.1016/j.gca.2012.11.048>, 2013.
- 658 Murray, R. H., Erler, D. V., and Eyre, B. D.: Nitrous oxide fluxes in estuarine environments: Response to global change,
659 <https://doi.org/10.1111/gcb.12923>, 2015.
- 660 NLWKN Bst. Aurich and Engels, A.: Abflussdaten Ems Ästuar (Pegeldaten Gandersum), 2021.
- 661 Ogilvie, B., Nedwell, D. B., Harrison, R. M., Robinson, A., and Sage, A.: High nitrate, muddy estuaries as nitrogen sinks: the
662 nitrogen budget of the River Colne estuary (United Kingdom), *Mar. Ecol. Prog. Ser.*, 150, 217–228,
663 <https://doi.org/10.3354/meps150217>, 1997.
- 664 Otte, S., Schalk, J., Kuenen, J. G., and Jetten, M. S.: Hydroxylamine oxidation and subsequent nitrous oxide production by the
665 heterotrophic ammonia oxidizer *Alcaligenes faecalis*, *Appl. Microbiol. Biotechnol.*, 51, 255–261,
666 <https://doi.org/10.1007/s002530051390>, 1999.



- 667 Papenmeier, S., Schrottke, K., Bartholomä, A., and Flemming, B. W.: Sedimentological and Rheological Properties of the
668 Water–Solid Bed Interface in the Weser and Ems Estuaries, North Sea, Germany: Implications for Fluid Mud Classification,
669 *J. Coast. Res.*, 289, 797–808, <https://doi.org/10.2112/JCOASTRES-D-11-00144.1>, 2013.
- 670 Pareja-Roman, L. F., Chant, R. J., and Sommerfield, C. K.: Impact of Historical Channel Deepening on Tidal Hydraulics in
671 the Delaware Estuary, *J. Geophys. Res. Oceans*, 125, e2020JC016256, <https://doi.org/10.1029/2020JC016256>, 2020.
- 672 Petersen, W., Schroeder, F., and Bockelmann, F.-D.: FerryBox - Application of continuous water quality observations along
673 transects in the North Sea, *Ocean Dyn.*, 61, 1541–1554, <https://doi.org/10.1007/s10236-011-0445-0>, 2011.
- 674 Quick, A. M., Reeder, W. J., Farrell, T. B., Tonina, D., Feris, K. P., and Benner, S. G.: Nitrous oxide from streams and rivers:
675 A review of primary biogeochemical pathways and environmental variables, *Earth-Sci. Rev.*, 191, 224–262,
676 <https://doi.org/10.1016/j.earscirev.2019.02.021>, 2019.
- 677 The R Stats Package, Version 4.0.2: <https://www.rdocumentation.org/packages/stats/versions/3.6.2/topics/prcomp>, last access:
678 29 January 2021.
- 679 Rhee, T. S., Kettle, A. J., and Andreae, M. O.: Methane and nitrous oxide emissions from the ocean: A reassessment using
680 basin-wide observations in the Atlantic, *J. Geophys. Res. Atmospheres*, 114, <https://doi.org/10.1029/2008JD011662>, 2009.
- 681 Robinson, A. D., Nedwell, D. B., Harrison, R. M., and Ogilvie, B. G.: Hypernutrified estuaries as sources of N₂O emission
682 to the atmosphere: the estuary of the River Colne, Essex, UK, *Mar. Ecol. Prog. Ser.*, 164, 59–71, 1998.
- 683 Röttgers, R., Heymann, K., and Krasemann, H.: Suspended matter concentrations in coastal waters: Methodological
684 improvements to quantify individual measurement uncertainty, *Estuar. Coast. Shelf Sci.*, 151, 148–155,
685 <https://doi.org/10.1016/j.ecss.2014.10.010>, 2014.
- 686 Sanders, T.: unpublished data.
- 687 Sanders, T. and Laanbroek, H. J.: The distribution of sediments and water column nitrification potential in the hyper-turbid
688 Ems estuary, *Aquat. Sci.*, 80, 2018.
- 689 Santoro, A. E. and Casciotti, K. L.: Enrichment and characterization of ammonia-oxidizing archaea from the open ocean:
690 phylogeny, physiology and stable isotope fractionation, *ISME J.*, 5, 1796–1808, <https://doi.org/10.1038/ismej.2011.58>, 2011.
- 691 GGally: Extension to “ggplot2”: <https://www.rdocumentation.org/packages/GGally/versions/1.5.0>, last access: 29 January
692 2021.
- 693 Schröder, F., Wiltshire, K. H., Klages, D., Mathieu, B., and Knauth, H. D.: Nitrogen and oxygen processes in sediments of the
694 Elbe Estuary, *Arch. Für Hydrobiol. Suppl.*, 110, 311–328, 1995.
- 695 Schuchardt, B. and Scholle, J.: Estuaries. Thematic Report No. 16, in: Marencic, H. and Vlas, J. de (Eds.). Quality Status
696 Report 2009. WaddenSea Ecosystem No. 25, Common Wadden Sea Secretariat, Trilateral Monitoring and Assessment Group,
697 Wilhelmshaven, Germany, 2009.
- 698 Seitzinger, S. P.: Denitrification in freshwater and coastal marine ecosystems: Ecological and geochemical significance,
699 *Limnol. Oceanogr.*, 33, 702–724, <https://doi.org/10.4319/lo.1988.33.4part2.0702>, 1988.
- 700 Sigman, D., Karsh, K., and Casciotti, K. L.: Ocean process tracers: Nitrogen isotopes in the ocean, *Encycl. Ocean Sci.*, 4138–
701 4153, 2009.



- 702 Sigman, D. M. and Fripiat, F.: Nitrogen isotopes in the ocean, *Encycl. Ocean Sci.*, 263–278, <https://doi.org/10.1016/B978-0-12-409548-9.11605-7>, 2018.
- 704 Sigman, D. M., Altabet, M., McCorkle, D., Francois, R., and Fischer, G.: The $\delta^{15}\text{N}$ of nitrate in the Southern Ocean: Nitrogen cycling and circulation in the ocean interior, *J. Geophys. Res.*, 105, 19599–19614, <https://doi.org/10.1029/2000JC000265>, 2000.
- 707 Sigman, D. M., Casciotti, K. L., Andreani, M., Barford, C., Galanter, M., and Böhlke, J. K.: A Bacterial Method for the Nitrogen Isotopic Analysis of Nitrate in Seawater and Freshwater, *Anal. Chem.*, 73, 4145–4153, <https://doi.org/10.1021/ac010088e>, 2001.
- 710 Stronge, W. B., Diaz, H. F., Bokuniewicz, H., Inman, D. L., Jenkins, S. A., Hsu, J. R. C., Kennish, M. J., Bird, E., Hesp, P. A., Crowell, M., Leatherman, S. P., Douglas, B., Rampino, M. R., Kennish, M. J., Healy, T. R., Gornitz, V., Doody, J. P., Kelletat, D., and Scheffers, A.: Estuaries, Anthropogenic Impacts, in: *Encyclopedia of Coastal Science*, edited by: Schwartz, M. L., Springer Netherlands, Dordrecht, 434–436, https://doi.org/10.1007/1-4020-3880-1_140, 2005.
- 714 Sutka, R. L., Ostrom, N. E., Ostrom, P. H., Breznak, J. A., Gandhi, H., Pitt, A. J., and Li, F.: Distinguishing Nitrous Oxide Production from Nitrification and Denitrification on the Basis of Isotopomer Abundances, *Appl. Environ. Microbiol.*, 72, 638–644, <https://doi.org/10.1128/AEM.72.1.638-644.2006>, 2006.
- 717 Talke, S. and de Swart, H. E.: Hydrodynamics and Morphology in the Ems/Dollard Estuary: Review of Models, Measurements, Scientific Literature, and the Effects of Changing Conditions, *Civ. Environ. Eng. Fac. Publ. Present.*, 87, 2006.
- 719 Talke, S. A., de Swart, H. E., and de Jonge, V. N.: An Idealized Model and Systematic Process Study of Oxygen Depletion in Highly Turbid Estuaries, *Estuaries Coasts*, 32, 602–620, <https://doi.org/10.1007/s12237-009-9171-y>, 2009.
- 721 Thornton, D. C. O., Dong, L. F., Underwood, G. J. C., and Nedwell, D. B.: *Marine Ecology Progress Series* 337:63, *Mar Ecol Prog Ser*, 63–77, 2007.
- 723 Tian, H., Xu, R., Canadell, J. G., Thompson, R. L., Winiwarter, W., Suntharalingam, P., Davidson, E. A., Ciais, P., Jackson, R. B., Janssens-Maenhout, G., Prather, M. J., Regnier, P., Pan, N., Pan, S., Peters, G. P., Shi, H., Tubiello, F. N., Zaehle, S., Zhou, F., Arneeth, A., Battaglia, G., Berthet, S., Bopp, L., Bouwman, A. F., Buitenhuis, E. T., Chang, J., Chipperfield, M. P., Dangal, S. R. S., Dlugokencky, E., Elkins, J. W., Eyre, B. D., Fu, B., Hall, B., Ito, A., Joos, F., Krummel, P. B., Landolfi, A., Laruelle, G. G., Lauerwald, R., Li, W., Lienert, S., Maavara, T., MacLeod, M., Millet, D. B., Olin, S., Patra, P. K., Prinn, R. G., Raymond, P. A., Ruiz, D. J., van der Werf, G. R., Vuichard, N., Wang, J., Weiss, R. F., Wells, K. C., Wilson, C., Yang, J., and Yao, Y.: A comprehensive quantification of global nitrous oxide sources and sinks, *Nature*, 586, 248–256, <https://doi.org/10.1038/s41586-020-2780-0>, 2020.
- 731 Tiedje, J. M.: Ecology of denitrification and dissimilatory nitrate reduction to ammonium, in: A.J.B. Zehnder (ed), *Environmental Microbiology of Anaerobes*, John Wiley and Sons, New York, 179–244, 1988.
- 733 Van Beusekom, J., Thiel, R., Bobsien, I., Boersma, M., Buschbaum, C., Dänhardt, A., Darr, A., Friedland, R., Kloppmann, M., Kröncke, I., Rick, J., and Wetzel, M.: Aquatische Ökosysteme: Nordsee, Wattenmeer, Elbeästuar und Ostsee, in: *Hamburger Klimabericht – Wissen über Klima, Klimawandel und Auswirkungen in Hamburg und Norddeutschland*, edited by: von Storch, H., Meinke, I., and Claußen, M., Springer, Berlin, Heidelberg, 89–107, https://doi.org/10.1007/978-3-662-55379-4_5, 2018.
- 738 Van Beusekom, J. E. E. and de Jonge, V. N.: The role of suspended matter in the distribution of dissolved inorganic phosphate, iron and aluminium in the ems estuary, *Neth. J. Aquat. Ecol.*, 28, 383–395, 1994.



- 740 Van Beusekom, J. E. E. and de Jonge, V. N.: Transformation of phosphorus in the wadden sea: Apatite formation, *Dtsch.*
741 *Hydrogr. Z.*, 49, 297–305, <https://doi.org/10.1007/BF02764040>, 1997.
- 742 Van Beusekom, J. E. E. and de Jonge, V. N.: Retention of Phosphorus and Nitrogen in the Ems Estuary, *Estuaries*, 21, 527–
743 539, 1998.
- 744 Van Beusekom, J. E. E., Carstensen, J., Dolch, T., Grage, A., Hofmeister, R., Lenhart, H., Kerimoglu, O., Kolbe, K., Pätsch,
745 J., Rick, J., Rönn, L., and Ruiters, H.: Wadden Sea Eutrophication: Long-Term Trends and Regional Differences, *Front. Mar.*
746 *Sci.*, 6, <https://doi.org/10.3389/fmars.2019.00370>, 2019.
- 747 Van Maren, D. S., Winterwerp, J. C., Wang, Z. Y., and Pu, Q.: Suspended sediment dynamics and morphodynamics in the
748 Yellow River, China, *Sedimentology*, 56, 785–806, <https://doi.org/10.1111/j.1365-3091.2008.00997.x>, 2009.
- 749 Van Maren, D. S., Winterwerp, J. C., and Vroom, J.: Fine sediment transport into the hyper-turbid lower Ems River: the role
750 of channel deepening and sediment-induced drag reduction, *Ocean Dyn.*, 65, 589–605, <https://doi.org/10.1007/s10236-015-0821-2>, 2015a.
- 752 Van Maren, D. S., van Kessel, T., Cronin, K., and Sittoni, L.: The impact of channel deepening and dredging on estuarine
753 sediment concentration, *Cont. Shelf Res.*, 95, 1–14, <https://doi.org/10.1016/j.csr.2014.12.010>, 2015b.
- 754 Voss, M., Baker, A., Bange, H. W., Conley, D., Cornell, S., Deutsch, B., Engel, A., Ganeshram, R., Garnier, J., Heiskanen,
755 A.-S., Jickells, T., Lancelot, C., McQuatters-Gollop, A., Middelburg, J., Schiedek, D., Slomp, C. P., and Conley, D. P.:
756 Nitrogen processes in coastal and marine ecosystems, in: *The European Nitrogen Assessment: Sources, Effects and Policy*
757 *Perspectives*, edited by: Bleeker, A., Grizzetti, B., Howard, C. M., Billen, G., van Grinsven, H., Erismann, J. W., Sutton, M. A.,
758 and Grennfelt, P., Cambridge University Press, Cambridge, 147–176, <https://doi.org/10.1017/CBO9780511976988.011>, 2011.
- 759 Wang, M., Moore, T. R., Talbot, J., and Riley, J. L.: The stoichiometry of carbon and nutrients in peat formation, *Glob.*
760 *Biogeochem. Cycles*, 29, 113–121, <https://doi.org/10.1002/2014GB005000>, 2015.
- 761 Wankel, S. D., Kendall, C., Francis, C. A., and Paytan, A.: Nitrogen sources and cycling in the San Francisco Bay Estuary: A
762 nitrate dual isotopic composition approach, *Limnol. Oceanogr.*, 51, 1654–1664, 2006.
- 763 Weiss, R. F. and Price, B. A.: Nitrous oxide solubility in water and seawater, *Mar. Chem.*, 8, 347–359,
764 [https://doi.org/10.1016/0304-4203\(80\)90024-9](https://doi.org/10.1016/0304-4203(80)90024-9), 1980.
- 765 de Wilde, H. P. and de Bie, M. J.: Nitrous oxide in the Schelde estuary: production by nitrification and emission to the
766 atmosphere, *Mar. Chem.*, 69, 203–216, [https://doi.org/10.1016/S0304-4203\(99\)00106-1](https://doi.org/10.1016/S0304-4203(99)00106-1), 2000.
- 767 Winterwerp, J. C., Wang, Z. B., van Braeckel, A., van Holland, G., and Kösters, F.: Man-induced regime shifts in small
768 estuaries—II: a comparison of rivers, *Ocean Dyn.*, 63, 1293–1306, <https://doi.org/10.1007/s10236-013-0663-8>, 2013.
- 769 Wong, W. W., Applegate, A., Poh, S. C., and Cook, P. L. M.: Biogeochemical attenuation of nitrate in a sandy subterranean
770 estuary: Insights from two stable isotope approaches, *Limnol. Oceanogr.*, 65, 3098–3113, <https://doi.org/10.1002/lno.11576>,
771 2020.
- 772 Wrage, N., Velthof, G. L., van Beusichem, M. L., and Oenema, O.: The role of nitrifier denitrification in the production of
773 nitrous oxide, *Soil Biol. Biochem.*, 33, 1723–1732, 2001.



- 774 Xia, X., Liu, T., Yang, Z., Michalski, G., Liu, S., Jia, Z., and Zhang, S.: Enhanced nitrogen loss from rivers through coupled
775 nitrification-denitrification caused by suspended sediment, *Sci. Total Environ.*, 579, 47–59,
776 <https://doi.org/10.1016/j.scitotenv.2016.10.181>, 2016.
- 777 Zhou, Y., Xu, X., Han, R., Li, L., Feng, Y., Yeerken, S., Song, K., and Wang, Q.: Suspended particles potentially enhance
778 nitrous oxide (N₂O) emissions in the oxic estuarine waters of eutrophic lakes: Field and experimental evidence, *Environ.*
779 *Pollut.*, 252, 1225–1234, <https://doi.org/10.1016/j.envpol.2019.06.076>, 2019.
- 780 Zhu, W., Wang, C., Hill, J., He, Y., Tao, B., Mao, Z., and Wu, W.: A missing link in the estuarine nitrogen cycle?: Coupled
781 nitrification-denitrification mediated by suspended particulate matter, *Sci. Rep.*, 8, [https://doi.org/10.1038/s41598-018-20688-](https://doi.org/10.1038/s41598-018-20688-4)
782 4, 2018.